



UNIVERSITY OF LEEDS

This is a repository copy of *Quantifying The Causes of Differences in Tropospheric OH within Global Models*.

White Rose Research Online URL for this paper:
<http://eprints.whiterose.ac.uk/112043/>

Version: Accepted Version

Article:

Nicely, JM, Salawitch, RJ, Canty, T et al. (13 more authors) (2017) Quantifying The Causes of Differences in Tropospheric OH within Global Models. *Journal of Geophysical Research: Atmospheres*, 122 (3). pp. 1983-2007. ISSN 2169-897X

<https://doi.org/10.1002/2016JD026239>

©2017 American Geophysical Union. All Rights Reserved. This is an author produced version of a paper published in *Journal of Geophysical Research: Atmospheres*. Uploaded with permission from the publisher.

Reuse

Unless indicated otherwise, fulltext items are protected by copyright with all rights reserved. The copyright exception in section 29 of the Copyright, Designs and Patents Act 1988 allows the making of a single copy solely for the purpose of non-commercial research or private study within the limits of fair dealing. The publisher or other rights-holder may allow further reproduction and re-use of this version - refer to the White Rose Research Online record for this item. Where records identify the publisher as the copyright holder, users can verify any specific terms of use on the publisher's website.

Takedown

If you consider content in White Rose Research Online to be in breach of UK law, please notify us by emailing eprints@whiterose.ac.uk including the URL of the record and the reason for the withdrawal request.



eprints@whiterose.ac.uk
<https://eprints.whiterose.ac.uk/>

Quantifying The Causes of Differences in Tropospheric OH within Global Models

Julie M. Nicely^{1,2,3}, Ross J. Salawitch^{1,4,5}, Timothy Canty⁴, Daniel C. Anderson⁴, Steve R. Arnold⁶, Martyn P. Chipperfield^{6,7}, Louisa K. Emmons⁸, Johannes Flemming⁹, Vincent Huijnen¹⁰, Douglas E. Kinnison⁸, Jean-François Lamarque⁸, Jingqiu Mao¹¹, Sarah A. Monks^{12,13}, Stephen D. Steenrod^{2,3}, Simone Tilmes⁸, Solene Turquety¹⁴

1. Department of Chemistry and Biochemistry, University of Maryland, College Park, Maryland, USA.
2. Atmospheric Chemistry and Dynamics Laboratory, NASA Goddard Space Flight Center, Greenbelt, Maryland, USA.
3. Universities Space Research Association, Columbia, Maryland, USA.
4. Department of Atmospheric and Oceanic Science, University of Maryland, College Park, Maryland, USA.
5. Earth System Science Interdisciplinary Center, University of Maryland, College Park, Maryland, USA.
6. Institute for Climate and Atmospheric Science, School of Earth and Environment, University of Leeds, Leeds, UK.
7. National Centre for Earth Observation, University of Leeds, Leeds, UK.
8. National Center for Atmospheric Research, Boulder, CO, USA.
9. European Centre for Medium-Range Weather Forecasts, Reading, UK.
10. Royal Netherlands Meteorological Institute, De Bilt, Netherlands.
11. Geophysical Institute and Department of Chemistry, University of Alaska Fairbanks, Fairbanks, Alaska, USA.
12. Chemical Sciences Division, Earth System Research Laboratory, National Oceanic and Atmospheric Administration, Boulder, Colorado, USA.
13. Cooperative Institute for Research in Environmental Sciences, University of Colorado Boulder, Boulder, Colorado, USA.
14. Laboratoire de Météorologie Dynamique, IPSL, Sorbonne Universités, UPMC Univ Paris 06, Paris, France.

Abstract

The hydroxyl radical (OH) is the primary daytime oxidant in the troposphere and provides the main loss mechanism for many pollutants and greenhouse gases, including methane (CH₄). Global mean tropospheric OH differs by as much as 80% among various global models, for reasons that are not well understood. We use neural networks (NNs), trained using archived output from eight chemical transport models (CTMs) that participated in the POLARCAT Model Intercomparison Project (POLMIP), to quantify the factors responsible for differences in tropospheric OH and resulting CH₄ lifetime (τ_{CH_4}) between these models. Annual average τ_{CH_4} , for loss by OH only, ranges from 8.0–11.6 years for the eight POLMIP CTMs. The factors driving these differences were quantified by inputting 3-D chemical fields from one CTM into the trained NN of another CTM. Across all CTMs, the largest mean differences in τ_{CH_4} ($\Delta\tau_{\text{CH}_4}$) result from variations in chemical mechanisms ($\Delta\tau_{\text{CH}_4} = 0.46$ years), the photolysis frequency (J) of O₃→O(¹D) (0.31 years), local O₃ (0.30 years), and CO (0.23 years). The $\Delta\tau_{\text{CH}_4}$ due to CTM differences in NO_x (NO+NO₂) is relatively low (0.17 years), though large regional variation in OH between the CTMs is attributed to NO_x. Differences in isoprene and J(NO₂) have negligible overall effect on globally averaged tropospheric OH, though the extent of OH variations due to each factor depends on the model being examined. This study demonstrates that NNs can serve as a useful tool for quantifying why tropospheric OH varies between global models, provided essential chemical fields are archived.

This article has been accepted for publication and undergone full peer review but has not been through the copyediting, typesetting, pagination and proofreading process which may lead to differences between this version and the Version of Record. Please cite this article as doi: 10.1002/2016JD026239

Key Points:

- 1) Factors responsible for OH and CH₄ lifetime differences between eight models are quantified using neural networks
- 2) O₃, the photolysis frequency (J) of O₃→O(¹D), CO, and chemical mechanism differences are main drivers of OH variations
- 3) H₂O & NO_x differences drive moderate OH variation on regional scale; isoprene & J(NO₂) differences have small role in driving OH variations

1 Introduction

The hydroxyl radical (OH) is the primary daytime oxidant in the troposphere [Levy, 1971] and is responsible for the breakdown of many pollutants and other atmospheric species of interest. Notably, the abundance and lifetime of methane (CH₄) are controlled by the global tropospheric OH concentration ([OH]^{TROP}). The chemistry of OH, however, is not easily modeled due to its numerous sources and sinks, rapid recycling in the presence of NO_x (=NO+NO₂), and non-linear chemical feedbacks that are not fully understood [Prather et al., 2001; Taraborrelli et al., 2012].

The inherent difficulty in modeling [OH]^{TROP} and CH₄ lifetime (τ_{CH_4}) on a global scale is evidenced by large differences in values of τ_{CH_4} reported by model intercomparison projects [Shindell et al., 2006; Fiore et al., 2009; Naik et al., 2013]. In general, lifetime is calculated as the atmospheric burden of a species divided by its total loss rate, but here, we use τ_{CH_4} to refer to the ratio of burden to loss of CH₄ with respect to reaction with tropospheric OH only. The four model intercomparison studies included in **Table 1**, not considering this study, show model spreads for τ_{CH_4} ranging from 62% [Fiore et al., 2009] to 84% [Shindell et al., 2006]. These spreads represent the difference between maximum and minimum values of τ_{CH_4} , divided by the multi-model mean.

The cause of model differences in τ_{CH_4} for the contemporary atmosphere is particularly critical to address because CH₄ is the second most important anthropogenic greenhouse gas. The lifetime of CH₄ factors directly into the calculation of the global

warming potential (GWP) of this compound [Table TS.2, IPCC, 2013]. Furthermore, models disagree on how τ_{CH_4} will evolve over the next century due to variations in atmospheric composition. Voulgarakis et al. [2013] found a multi-model mean change in τ_{CH_4} of $+8.5 \pm 10.4\%$ between year 2000 and 2100, for simulations conducted using 14 models driven by the Representative Concentration Pathway (RCP) 8.5 greenhouse gas emissions scenario. Of the 14 models analyzed, three yielded decreases in τ_{CH_4} , for year 2100 relative to year 2000, while another three yielded increases in τ_{CH_4} that exceed $+25\%$. This level of disagreement illustrates that the effect of climate change on the future oxidizing capacity of the troposphere is highly uncertain, due to a large range of possible future emission scenarios that will alter atmospheric composition as well as variations in model behavior with respect to OH. The path to reducing this uncertainty lies in first accurately assessing why present-day $[\text{OH}]^{\text{TROP}}$ and τ_{CH_4} differ among models.

Another challenge to our understanding of $[\text{OH}]^{\text{TROP}}$ is the persistent discrepancy between τ_{CH_4} values calculated by models and those based on observations. Measurements of the temporal evolution of the global mean abundance of methyl chloroform (MCF: CH_3CCl_3) as well as the global emission rate of MCF are frequently used to infer the abundance of $[\text{OH}]^{\text{TROP}}$ and hence τ_{CH_4} . Prinn et al. [2005] estimated a mean chemical τ_{CH_4} of $10.2^{+0.9}_{-0.7}$ years for the 1978–2004 period following this method. Prather et al. [2012] adopted a more sophisticated approach, considering more terms for loss of MCF than prior studies, and estimated τ_{CH_4} to be 11.2 ± 1.3 years for year 2010. IPCC [2013] (see Section 8.SM.2) uses the Prather et al. value of τ_{CH_4} for its latest set of GWP estimates due to CH_4 . For comparison, the multi-model mean values for present-day τ_{CH_4} calculated by Shindell et al. [2006], Fiore et al. [2009], and Naik et al. [2013] are 9.72 ± 1.70 , 10.19 ± 1.72 , and 9.7 ± 1.5 years, respectively. Uncertainties in the empirical estimates of τ_{CH_4} include potential stockpiling of MCF and resulting inaccuracies in assumed emissions [Krol and Lelieveld,

2003], ocean outgassing of MCF at high latitudes [Wennberg et al., 2004], and uncertainty in the rate constants for the OH+MCF and OH+CH₄ reactions [Prather et al., 2012]. Given that CH₄ is such a potent greenhouse gas and that the sign of future changes in τ_{CH_4} is uncertain [Voulgarakis et al., 2013], the low bias in modeled τ_{CH_4} relative to the recent empirical estimate provided by Prather et al. [2012] is important to understand and eventually resolve.

There have been three recent attempts to assess our understanding of tropospheric OH based on observations. Strode et al. [2015] used satellite observations of CO to analyze the hemispheric biases in modeled OH. That study investigated possible solutions to bring the modeled ratio of Northern Hemisphere (NH) to Southern Hemisphere (SH) burdens of OH (greater than 1 in most models [Mao et al., 2013a; Naik et al., 2013]) into better agreement with observation-based estimates of the NH:SH ratio (almost exactly 1 according to recent studies [Krol and Lelieveld, 2003; Patra et al., 2014]). The ratio of NH:SH burdens of OH is a metric often used to evaluate τ_{CH_4} because its variation between models can indicate whether discrepancies are due to hemisphere-specific processes, such as anthropogenic emissions concentrated in the NH, or processes that occur equally in both hemispheres, such as loss by longer-lived, well-mixed species including CH₄. While the hemispheric gradient of OH is not directly constrained by observations, latitudinal gradients of species primarily lost by OH (e.g., CO and MCF) are well established from satellite, aircraft, and ground-based measurements. Strode et al. [2015] found that reducing NH OH brought the modeled latitudinal gradient of CO into better agreement with observations. Further simulations conducted by Strode et al. were unable to attribute the large ratio of NH:SH OH in the model to known model deficiencies in O₃ and H₂O. The second observation-based study by Patra et al. [2014] used ground-based measurements of MCF and a chemical transport model (CTM) to estimate the ratio of NH:SH burdens of OH as 0.97 ± 0.12 . Further, they attributed ratios greater than 1 in other models to likely overestimates in emissions of reactive species such as

NO_x. In a third study, Nicely et al. [2016] found that OH inferred from observations of precursors in the tropical western Pacific tended to exceed concentrations of OH calculated by global CTMs by up to 20%. For this region during January–February 2014, CTM underestimates of NO_x and HCHO were the primary drivers of underestimated OH. Conversely, underestimates in CTM acetaldehyde (CH₃CHO) relative to observations resulted in the magnitude of the OH sink being underestimated in the CTM at low altitudes, partially compensating for the underestimated NO_x and HCHO sources. Therefore, it is unclear from these attempts to constrain OH using observations why models are presently overestimating the oxidizing capacity of the troposphere, relative to the CH₄ lifetime based on MCF inversion studies.

The non-linear chemical response of OH to changes in sources and sinks, and the co-dependencies between many drivers of OH, present a challenge to modeling [OH]^{TROP} on a global scale [Spivakovsky et al., 1990; Duncan et al., 2000]. A thorough investigation of multi-model differences in τ_{CH_4} would require methodical examination of the complete chemical mechanisms of each participating model, which is an unreasonable expectation. Other methods such as Gaussian process emulation aim to quantify and attribute sources of model uncertainty based on performing multiple simulations with inputs spanning reasonable parameter ranges in a computationally efficient manner [e.g. Lee et al., 2012; Lee et al., 2016]. However, modeling tropospheric chemistry involves a multitude of parameters, many of them highly uncertain, and re-running even a single CTM with perturbed inputs is time-consuming and labor-intensive. In this study, we use the computational power of neural networks (NNs) [Jain et al., 1996; Gardner and Dorling, 1998; Heaton, 2011; Allison, 2015] to mimic the behavior of the chemical mechanism of each of eight CTMs and reproduce its global OH output. The parallel computation method employed by NNs allows for the fitting of non-linear systems using codependent variables as inputs. We use NNs with output

generated for the POLARCAT (Polar Study using Aircraft, Remote Sensing, Surface Measurements and Models, of Climate, Chemistry, Aerosols and Transport) Model Intercomparison Project (POLMIP) [Emmons et al., 2015] to quantify the effect of the input parameters in driving differences in τ_{CH_4} .

2 Method

2.1 POLMIP CTMs

The POLMIP intercomparison project [Emmons et al., 2015] was designed to take advantage of the POLARCAT [Law et al., 2014] suite of observations taken in 2008. While the POLARCAT measurements focus on study of the Arctic troposphere, POLMIP includes model simulations with global coverage. Simulations were performed with a common emissions inventory (specifying separately emissions from anthropogenic, biomass burning, biogenic, soil, ocean, and volcano sources) for January to December 2008 with output provided as monthly means for each month (see Emmons et al. [2015] for further detail). However, emissions of some hydrocarbon species within the GEOS-Chem model vary significantly from those recommended. Participating models were run as CTMs, meaning they used winds and temperatures based on analyzed meteorological fields. As such, there was general consistency in the meteorological variables among the models, though some additional meteorological fields (e.g., water vapor, clouds, convection) were input to some models whereas these quantities were calculated internally in others. Each model provided monthly mean output for many chemical, physical, and radiative variables using the standard chemistry and deposition schemes of each group. Only those models that output fields with global coverage are included in this study. Since this analysis relies on relative differences among models, output from only one (Version 4) of two available versions of CAM-Chem is considered, to eliminate a small bias due to use of output from two highly similar models.

The eight models participating in this analysis are listed in **Table 2**. Treatment of aerosols, the tropospheric chemistry scheme implemented, inclusion of stratospheric chemistry, and parameterization of lightning NO_x ($\text{NO}+\text{NO}_2$) vary between these models (see Emmons et al. [2015] for further detail). For instance, the GEOS-Chem CTM employed a heterogeneous uptake pathway for hydroperoxy radical (HO_2) on aerosols that is unique among the POLMIP CTMs [Mao et al., 2013a]. CAM-Chem, GEOS-Chem, GMI, and MOZART-4 use GEOS-5 meteorology [Molod et al., 2012], while TM5, C-IFS, TOMCAT and LMDz-INCA use ERA-interim meteorology [Dee et al., 2011]. Latitude \times longitude grids and number of vertical levels for each model are listed in Table 2. However, because of the fine spatial resolution of the C-IFS model output, the computer used for the NN analysis did not have enough memory to train a NN using the raw archived output. Therefore, output from C-IFS was bilinearly interpolated to a $2.0^\circ \times 2.5^\circ$ latitude/longitude grid for training of the NN.

Given that emissions of chemical species, atmospheric transport fields, and meteorology should be relatively consistent between the various CTM simulations, differences in τ_{CH_4} likely arise from variations in the OH precursor and sink fields, the radiative conditions, and the chemical mechanisms inherent to each model. It is possible that differences in certain meteorological parameters that are not necessarily consistent between models (e.g. clouds) also influence OH indirectly through their effect on photolysis frequencies [e.g. Rohrer and Berresheim, 2006; Voulgarakis et al., 2009]. Additionally, OH precursors such as NO_x can be both directly emitted as well as generated by lightning, which is parameterized in a manner individual to each model. However, we focus on the factors that directly affect OH chemistry. To answer whether model differences in those factors are driven by emissions, chemistry, deposition, or the radiative environment necessitates the archiving of output fields that were not available for this study. Additionally, to properly

evaluate the role of fast chemistry (i.e., OH recycling from HO₂ and alkylperoxy radicals, RO₂), additional chemical fields at higher temporal frequency must also be archived. Here, we use NNs to quantify the drivers of inter-model differences in τ_{CH_4} by swapping monthly mean OH precursor and sink fields from one model into the NNs of other models.

For our analysis of CTM output, values of τ_{CH_4} were calculated as the total tropospheric burden of CH₄ divided by the CH₄ loss rate:

$$\tau_{\text{CH}_4} = \frac{\sum M_{\text{air}} \times \chi_{\text{CH}_4}}{\sum [\text{OH}] \times k_{\text{OH}+\text{CH}_4} \times M_{\text{air}} \times \chi_{\text{CH}_4}} \quad (1)$$

where M_{air} is the mass of air within a grid box, brackets denote number density, χ denotes mixing ratio, $k_{\text{OH}+\text{CH}_4}$ is the reaction rate constant for the OH+CH₄ reaction calculated for each grid box temperature, and summations are performed over all tropospheric model grid boxes. In this formulation of lifetime calculation, the numerator represents the total burden of CH₄ in kg, while the denominator represents the loss of CH₄ by reaction with tropospheric OH in units of kg s⁻¹. Tropopause pressures were calculated for each model by using vertical profiles of O₃ and CO mixing ratios to identify a chemical tropopause, following the method of Pan et al. [2004]. **Figure 1** shows the τ_{CH_4} evaluated using Eq. 1 for each month for the eight CTMs analyzed here. The LMDz-INCA model generally exhibits the longest τ_{CH_4} (i.e. lowest values of tropospheric OH), with an annual mean τ_{CH_4} of 11.6 years. The TOMCAT model has the shortest τ_{CH_4} , with an annual average of 8.0 years.

The annual average values of τ_{CH_4} from the eight CTMs are listed in **Table 3**. The inter-model spread of τ_{CH_4} for these eight CTM simulations is 39%, found by taking the difference between the maximum and minimum values, and dividing by the multi-model mean. This spread is smaller than reported in other comparisons, likely because these other studies involve a larger number of CTMs and more extreme outliers of τ_{CH_4} (τ_{CH_4} as low as

6.2 years in Fiore et al. [2009] and as high as 15 years in Shindell et al. [2006]). Given the nature of our study, we are only able to use output from CTMs that archive global, monthly fields of a large number of chemical constituents. Most importantly, we note that all but one value of τ_{CH_4} given in Table 3 are shorter than the value of 11.2 years used by IPCC [2013] for the computation of the GWP of CH_4 .

2.2 Neural Network Training

Neural networks can be thought of as an advanced parameterization method well suited to model non-linear systems. Applications include problems as varied as speech recognition, data mining, and stock market forecasting [Jain et al., 1996]. Others in the atmospheric science community have used NNs to forecast O_3 air quality events [Comrie, 1997], improve satellite retrievals of aerosol optical depth [Lary et al., 2009], and estimate reaction rate constants and dissociation energies of atmospherically relevant species not easily measured experimentally [Gramatica et al., 1999; Urata et al., 2002; Urata et al., 2003; Allison, 2015]. As far as we are aware, NNs have not yet been applied to diagnose and improved tropospheric chemical processes within global models.

In this study, NNs were developed individually for each CTM, one for each of four months to span the seasons (i.e., January, April, July, and October) using the Matlab Neural Network Toolbox Version 8.0.1 available from MathWorks [Beale et al., 2013]. Each NN was trained to reproduce the 3-D monthly mean field of OH mixing ratio from the CTM; Section 3.1 presents metrics on the performance of all NNs. Inputs were chosen based on their direct influence on OH chemistry. Here we used monthly mean averages of 11 variables: volume mixing ratios of H_2O , O_3 , NO_x , CO, CH_4 , and isoprene, along with photolysis frequencies $J(\text{O}_3 \rightarrow \text{O}(^1\text{D}))$ and $J(\text{NO}_2)$ (units of s^{-1}) and physical parameters latitude, pressure (units of hPa), and temperature (units of K). These inputs were chosen

based on the OH parameterization originally developed by Spivakovsky et al. [1990] and explicitly listed in Table 1 of Duncan et al. [2000]. We used all of the parameters from the Duncan et al. parameterization that were archived for all POLMIP model simulations with the exception of ethane (C_2H_6) and propane (C_3H_8). These species were not included here because their emissions were commonly prescribed for all models and they account for a small percentage of total OH reactivity. The addition of C_2H_6 and C_3H_8 to the calculation of OH reactivity results in an increase of less than 0.4% of the total OH reactivity on a global mean basis for all POLMIP CTMs (**Figures S1** and **S2**; Lelieveld et al. [2016]). Additionally, we use monthly mean fields of $J(O_3 \rightarrow O(^1D))$ and $J(NO_2)$ as inputs to the NN, rather than the parameters surface and cloud albedo, declination angle, and overhead O_3 column that appear in Table 1 of Duncan et al. [2000]. The availability of these two photolysis frequencies in the POLMIP archive provides a more direct connection to tropospheric OH than the photolytically related parameters in their table. Because surface CH_4 is set as a boundary condition in the POLMIP model simulations, and little overlap exists between ranges of CH_4 values for some of the models as shown in **Figure S3**, we input CH_4 for each grid box as the ratio of model CH_4 mixing ratio to the maximum tropospheric value present in a given model for that particular month.

Neural networks can be configured with many different architectures and degrees of processing power [Gardner and Dorling, 1998]. We found the architecture that struck the best balance between being computationally efficient and accurate in reproducing the OH fields for a given CTM was the feed-forward NN (meaning that processing only occurs in a forward direction, as opposed to cyclically as occurs in other architectures) consisting of two hidden layers (**Figure 2**). Following extensive testing of various configurations, we selected NNs containing 15 nodes (represented by the blue circles in Figure 2) per layer for most of the CTMs. However, we extended the NNs for TOMCAT, C-IFS, and GEOS-Chem to

contain 30 nodes per layer due to larger errors evident in OH fields generated by the less powerful NN architecture. This may be due to stronger influence of other chemical species on the chemistry of OH in these models, preventing our selection of NN inputs from fully explaining model variations in OH. Alternatively, for C-IFS, it is possible that interpolation to a coarser spatial grid could distort the chemical equilibria expressed between species. In order to reproduce OH from each model with comparable accuracy, we created NNs that are more computationally expensive for these three CTMs. The training method used here is similar to methods found in Lary et al. [2009] and Allison [2015].

Here we provide further detail of our implementation of the NN. At each node, a hyperbolic tangent activation function (see bottom of Figure 2) is performed on the linear combination of each input multiplied by a unique weighting (represented by the grey arrows in Figure 2). The Levenberg-Marquardt algorithm [Heaton, 2011] was used to adjust NN weights during training, based on the second derivatives of the errors of the simulated OH mixing ratios. Of all the tropospheric grid points output for a single model month, 80% of those were used to adjust weights during training of the NN, 10% were used to evaluate errors and determine a stopping point during training, and 10% were used as an independent validation of the NN post-training, following the method of Lary et al. [2009].

The end of NN training was determined by calculating the mean squared error (MSE) between CTM OH and OH calculated by the NN for 10% of the data points not used to adjust NN weights. In the event that the MSE increased six iterations in a row, following six sets of weight adjustments, training was stopped and the NN weights prior to the error increase were saved. In other words, the NN weightings that minimize a cost function and cannot be adjusted to decrease errors further are saved. Upon completion of NN training, the remaining 10% of data points are used to validate the final weights by regressing OH calculated by the

NN versus CTM OH. The training process is repeated several times to identify the NN weights that maximize the r^2 value of this regression.

Upon successful training of NNs for each CTM, the performance of each NN was evaluated by calculating tropospheric OH mass columns and τ_{CH_4} for the NN-simulated fields of OH and comparing these NN-derived quantities to the values derived from the CTM output. Tropospheric mass columns were calculated by vertically integrating the mass of OH in the column from the surface to the tropopause then normalizing by the base area of the surface grid box. **Figure 3** provides an example of the OH mass column distribution we see from GMI for the month of July and representative NN performance. Figures 3a and 3b show OH mass columns from the GMI CTM and NN, respectively. The difference in the OH mass columns, NN–CTM, is shown in Figure 3c. While differences on the order of $\pm 5\%$ between the NN and CTM exist in some locations, the OH mass column distributions in Figures 3a and 3b are nearly visually identical. NN performance is further quantified and discussed for all CTMs in Section 3.1.

2.3 Quantifying Precursor Effects on OH

Once established, NNs for each CTM were then used to quantify the effect on τ_{CH_4} of replacing one of the OH precursor fields (e.g., the distribution of O_3) with that from another CTM. This was done by running the NN with inputs from the parent CTM, except for a single input field taken from another CTM. This “swapped” input was interpolated to the native spatial grid of the parent CTM and run through a series of checks, to prevent a value outside of the range over which the NN was trained from being passed to the NN. The latter step prevents the NN from extrapolating outside of the “trained range” of an input variable. Such extrapolation, which we have fastidiously avoided in the results herein, would result in anomalous values of OH being output, even for a well-trained NN.

Here we describe our method for handling situations when the swapped variable from one NN is outside the trained range of another NN, which we term “extrapolation control”. To test the effect of MOZART-4 CO on the value of OH output by the GMI NN, each MOZART-4 CO value is compared to ranges of CO mixing ratios acceptable for the values of GMI O₃, CH₄, isoprene, etc. that co-existed with this value of CO during training. In other words, if the MOZART-4 CO value was indicative of pollution, while the other GMI variables indicate clean conditions, the substituted CO value will likely be too high for the NN in an otherwise clean chemical regime. In this case, the CO value would be revised down to the highest “acceptable” mixing ratio of CO, over which the NN was trained for clean conditions. Our extrapolation control method is accomplished by compiling a series of reference matrices for each CTM and checking against the appropriate matrix whenever a variable substitution is conducted.

After running a NN with an input field substituted from another CTM, new values of tropospheric OH mass column and τ_{CH_4} were calculated from the output OH mixing ratios. The change in both, relative to the parent NN base run, is attributed to the substituted variable. These swaps were performed for all chemical and radiative variables, as well as temperature, between all models.

2.4 Evaluation against box model

A box model is used to determine whether the chemical mechanisms within individual CTMs are also responsible for differences in $[\text{OH}]^{\text{TROP}}$ and τ_{CH_4} . The box model employed is the Dynamically Simple Model of Atmospheric Chemical Complexity (DSMACC) [Emmerson and Evans, 2009], operating with the Master Chemical Mechanism (MCM) [Jenkin et al., 1997; Saunders et al., 2003] version 3.3.1 [Jenkin et al., 2015]. Each of the NN input values is determined by finding an average value representative of a particular

geographic region for all tropospheric pressure levels. Hourly values of $J(\text{NO}_2)$, $J(\text{O}_3 \rightarrow \text{O}^1\text{D})$, and NO from CAM-Chem, GMI, and LMDz-INCA, are used to scale monthly mean output from all eight CTMs, used in the NNs, to an instantaneous noon-time value that is then input to the box model, following the method of Nicely et al. [2016]. The hourly output necessary to do this is only available from the three CTMs noted for April along with June-July; we perform the box model analysis only for the springtime month. All other species were constrained in the box model using the monthly mean NN input value. Monthly means of the additional species ethane (C_2H_6), propane (C_3H_8), acetone (CH_3COCH_3), acetaldehyde (CH_3CHO), and formaldehyde (HCHO) from each CTM are also input to the box model (with the exception of acetone from C-IFS, which was not archived). This enables the box model, which explicitly represents the chemistry of OH production and loss (as opposed to the NN method that treats isoprene as a proxy for other VOCs that also affect OH), to accurately evaluate how purely chemical mechanism-related differences may be influencing OH. The box model is run to diurnal steady state, and mixing ratios of OH output from these runs were averaged to obtain a 24-hour mean, which are directly compared to CTM monthly mean values.

We have conducted box model evaluations of the CTM chemical mechanisms for 4 distinct geographic regions shown in **Figure 4**: the Eastern Pacific, Atlantic, Africa, and Western Pacific. Figure 4 also shows tropospheric OH mass columns for the month of April calculated using output from the TOMCAT (top) and LMDz-INCA (bottom) CTMs, which give the shortest and longest values of τ_{CH_4} , respectively, among the POLMIP models. We focus this analysis on regions with relatively low NO_x and low VOCs due to our ability to reproduce CTM OH in these chemical regimes with reasonable accuracy using the box model. Large discrepancies between OH calculated by the box model and the CTMs in regions of high NO_x and/or high VOCs, such as over the Amazon, are likely due to the

influence on OH from other species (e.g., methanol, monoterpenes) not output by the CTMs for the POLMIP archive. Differences between the CTM and box model chemical mechanisms that are particularly important for these high NO_x and/or high VOC regimes could also influence the box model OH discrepancies. Results for the box model analysis are discussed in Section 3.4 below.

3 Results

3.1 Neural Network Performance

The NNs reproduced OH mixing ratios from the CTMs and resulting tropospheric OH mass columns with good accuracy. **Figure S4** shows tropospheric column mass differences between the NN and each CTM for July, analogous to Figure 3c. Generally the NNs perform well for most regions, with simulated column mass OH within $\pm 5\%$ of the CTM values. Additionally, the mean squared error (MSE) metric by which the NNs were validated generally fell below 1.0×10^{-3} , which indicates very good performance. The NNs for C-IFS and GEOS-Chem, however, exhibited errors higher than this threshold for at least one of the four months for which NNs were trained (0.0012 in January for C-IFS; 0.0019, 0.0019, and 0.0012 in January, April, and July, respectively, for GEOS-Chem), despite use of a more powerful NN architecture. NN performance also displayed a seasonal dependence, with all producing highest MSE values in January and lowest MSE values in October or April. Finally, the most important quantity, τ_{CH_4} , which reflects global tropospheric OH in each CTM, is reproduced well by the NNs. The largest error in τ_{CH_4} shown in Figure S4, 0.019 years or 0.25%, results from the NN for TM5. The extremely high accuracy for τ_{CH_4} results from the tendency of overestimates of OH in some geographic regions to be balanced by underestimates in other regions (i.e., over- and underestimates of OH tend to cancel, when τ_{CH_4} is examined).

The spatial distribution of the difference between NN and CTM tropospheric OH mass column indicates that NN errors are most concentrated either over continents or in oceanic regions affected by continental outflow. This may be due to the influence of an emission source that leads to a unique set of chemical conditions for which the NN could not be sufficiently trained. In addition, monthly mean averages of the parameters used as input to the NN may not be able to represent the non-linearity of the chemical conditions in the actual POLMIP CTM simulation that led to a particular monthly mean value of OH, at a specific model grid point. Regardless of these localized errors, the NNs are able to reproduce τ_{CH_4} values for their respective CTMs to within ± 0.02 years and the worst performing NN (GEOS-Chem), based on MSE, reproduces a τ_{CH_4} 0.012 years higher than the native CTM. As such, the NN error in calculating τ_{CH_4} is less than 0.25%.

3.2 Individual Precursor Analysis

Each input variable was “swapped” between all models for a given month, allowing the impact on OH to be examined for each of the primary parameters that affect OH. Comparisons of tropospheric OH mass differences due to CO, NO_x, J(O₃→O¹D), and J(NO₂) swaps between CAM-Chem and GEOS-Chem are shown in **Figure 5**, and CH₄, isoprene, H₂O, and O₃ swaps in **Figure 6**. We show OH differences from these two CTMs because they are representative of results from most other model pairings, in which CH₄ lifetimes of the parent CTMs vary by ~1 year. The order of variable swaps listed here and shown in the two figures is determined by the mean absolute value of $\Delta\tau_{\text{CH}_4}$, the change in τ_{CH_4} resulting from the performed swap. The first four variables, CO, NO_x, J(O₃→O¹D), and J(NO₂), influence the largest changes in τ_{CH_4} for this model pair. Color bars for the pair of plots on the left and right of each row are mirror images of each other, designed to represent the fact that decreases in OH in one model for a variable swap should be accompanied by increases in

OH when the swap occurs in the opposite direction. Values of $\Delta\tau_{\text{CH}_4}$ are also imprinted on each panel of Figures 5 and 6. As with the spatial distribution of OH mass differences, values of $\Delta\tau_{\text{CH}_4}$ shown in the left and right hand side of each row are expected to be opposite in sign and of roughly the same magnitude. Inspection of these figures shows this expectation is generally met, further validating proper behavior of the NNs.

The primary driver of differences in τ_{CH_4} between CAM-Chem and GEOS-Chem is CO. Widespread decreases in OH are found by the CAM-Chem NN as a result of using CO from GEOS-Chem, which is generally higher than CO from CAM-Chem (Figure 5b). This results in a net increase in τ_{CH_4} of 0.48 years. When the swap of CO occurs in the other direction; i.e., use of CO from CAM-Chem in the GEOS-Chem NN, we see a widespread increase in OH corresponding to a decrease in τ_{CH_4} of 0.75 years (Figure 5a). The direction of change agrees with expectations, since CO from CAM-Chem is generally lower than CO from GEOS-Chem as shown in **Figure S5**. The visual similarity of the colors on the left hand plots to those on the right hand plots, for each row, confirms the NNs are behaving in a reasonable manner. Despite a common emissions inventory being provided, in the case of GEOS-Chem, some hydrocarbon emissions are very different from those specified [Emmons et al., 2015]. Secondary production of CO from oxidation of these hydrocarbons could play a large role in explaining the strong CO variations among models. Whatever the cause, the largest differences in τ_{CH_4} and OH between GEOS-Chem and CAM-Chem are driven by differences in the fields of CO.

The effect of swapping NO_x between GEOS-Chem and CAM-Chem within the respective NNs (Figures 5c and 5d) highlights large differences in OH, particularly over continental source regions. While the POLMIP project specified a common emissions inventory for use by all CTMs, it is possible that the implementation of the inventory in the various models differs or that nitrogen chemistry (including sequestration of NO_x to reservoir

species such as peroxyacetyl nitrate (PAN)) evolves in a different manner following emission, resulting in moderately varied fields of NO_x among the eight CTMs as shown in **Figure S6**. Variations in CTM parameterizations of lightning NO_x could also account for the large differences in OH resulting from the NO_x swaps. Murray et al. [2013] noted the importance of lightning NO_x for accurately modeling the interannual variability of OH. Interestingly, while there are considerable regional differences in the tropospheric mass of OH resulting from the swap of NO_x in the NN analysis, the resulting difference in τ_{CH_4} is modest. Regions of enhanced OH in one region (Central America) tend to be offset by regions of suppressed OH in other areas (India and SE Asia).

Differences in OH driven by photolysis frequencies ($J(\text{O}_3 \rightarrow \text{O}(^1\text{D}))$) in Figures 5e and f and $J(\text{NO}_2)$ in Figures 5g and h exhibit more global uniformity than differences driven by NO_x and isoprene. Variations in $J(\text{O}_3 \rightarrow \text{O}(^1\text{D}))$ generally arise from differences in overhead O_3 column, which exhibit considerable range among these eight CTMs. Only two of the models (GMI and CAM-Chem) include interactive stratospheric chemistry. The others constrain stratospheric O_3 concentrations to climatological mean values. **Figure S7** shows the large variations in the dependence of $J(\text{O}_3 \rightarrow \text{O}(^1\text{D}))$ on overhead O_3 column among the eight CTMs. The CTMs also calculate photolysis frequencies using differing methods, as detailed in **Table S1**. Strong differences in cloud coverage [Emmons et al., 2015] are also likely to play a role in causing photolysis frequency variations between models. Despite use of one of two common sources of meteorological fields (either GEOS-5 or ERA-interim), models may either use H_2O and cloud fields from that source directly or calculate their own fields based on surface fluxes and model physics. As a result, model fields of H_2O (**Figure S8**) and clouds vary considerably as shown in Emmons et al. [2015]. The differences in $J(\text{O}_3 \rightarrow \text{O}(^1\text{D}))$ between CAM-Chem and GEOS-Chem are consistent with the direction of change in OH shown in Figures 5e and 5f: i.e., GEOS-Chem exhibits lower values of

$J(\text{O}_3 \rightarrow \text{O}(^1\text{D}))$) than CAM-Chem, resulting in an increase in OH upon swapping CAM-Chem $J(\text{O}_3 \rightarrow \text{O}(^1\text{D}))$ into the GEOS-Chem NN. The origin of differences in $J(\text{NO}_2)$, on the other hand, is primarily due to various model representations of cloud coverage and surface albedo. Variations in the CTM fields of overhead O_3 and clouds are manifest on a global scale, resulting in differences in OH due to photolysis frequencies that have comparable magnitude across continents and oceans. Even so, OH features are still distinguishable, such as the strong increase in OH over Indonesia in the CAM-Chem NN due to $J(\text{NO}_2)$ (Figure 5h). Since not all models have output a variable containing information on cloud coverage for the POLMIP archive, we can only surmise that the CAM-Chem treatment of clouds over Indonesia differs from that within GEOS-Chem.

Figure 6 shows the impacts on OH of swapping the variables that have the least impact on τ_{CH_4} between GEOS-Chem and CAM-Chem: CH_4 , isoprene, H_2O , and O_3 . The result of swapping CH_4 between the two CTMs (Figures 6a and 6b) reveals a shortcoming in the NN approach when one model uses a fixed 3-D field of an input parameter. In this case, the use of constant CH_4 mixing ratios throughout the troposphere in GEOS-Chem results in an inability of the NN to evaluate the effect of other CH_4 values (Figure 6a) for reasons explained below (i.e. the paragraph that begins “An extreme case”). The CAM-Chem NN, on the other hand, suggests a change in τ_{CH_4} of -0.14 years resulting from the use of CH_4 from the GEOS-Chem CTM, largely due to increases in OH throughout most of the tropics. Swaps of isoprene (Figures 6c and 6d) show almost complete localization of resulting OH differences to continental source regions, due to the short lifetime of isoprene. As for NO_x , the isoprene driven variations in OH could result either from differences in the implementation of isoprene emissions or from alternate representations of the impact on OH of isoprene oxidation, an area of active current research [Mao et al., 2013b].

We also show results for the swapping of inputs between the LMDz-INCA and TOMCAT NNs (**Figures S9** and **S10**). These two CTMs exhibit the largest difference in τ_{CH_4} ; LMDz-INCA has the longest lifetime (11.6 years) whereas TOMCAT has the shortest value (8.0 years) (Table 3). While some of the variable swaps indicate large values of $\Delta\tau_{\text{CH}_4}$ (H_2O in Figure S10e and f; NO_x in S9c and d), the sum of the eight values of $\Delta\tau_{\text{CH}_4}$ for swapping in one direction (0.77 years for left hand panels) or the other direction (-1.28 years) does not account for the 3 year difference in τ_{CH_4} between these two CTMs for the month of July. We conclude therefore that a considerable portion of the variation in OH between LMDz-INCA and TOMCAT is due to differences in the chemical mechanisms within these two CTMs, which is examined further in Section 3.4. One indicator of this may be the very different responses to CH_4 being swapped between these two CTMs. Whereas we generally expect an OH increase in one model to be accompanied by an OH decrease in the other, we instead see widespread OH increases in both models except for OH decreases localized over the tropical continents in the TOMCAT NN. TOMCAT generally has higher CH_4 than LMDz-INCA, so the LMDz-INCA NN indicates that OH concentrations increase due to the input of higher CH_4 . This response differs from that of the TOMCAT NN, which shows OH increasing as a result of lower CH_4 . It is these variations in OH responses that reveal the likely presence of important chemical mechanism differences.

Upon examination of the 2,016 tropospheric mass OH difference plots generated by our NN analysis (eight models combined with seven possible pairs, for the eight variables shown above plus the ninth variable temperature, times four months), it is important to recognize several points. As noted above, the pairings of tropospheric column mass OH difference plots and $\Delta\tau_{\text{CH}_4}$ values for swaps of precursor fields in both directions are expected to demonstrate some level of visual and quantitative symmetry, and this is generally the case. There are, however, instances where this symmetry is lacking. The cause of this may be

twofold. First, the chemical mechanism inherent to the respective CTMs may exhibit varying responses to the variable being swapped. The second cause may be due to the extrapolation control method used to confine substituted variables to the range of values for which each NN was trained. If one CTM produces a wide range of tropospheric values, e.g. for CH₄, while a second confines the species to a very narrow range, the swap in CH₄ values between the NNs of the two CTMs will be asymmetric. Extrapolation control will allow the NN of the first CTM to test the full range of the field of CH₄ generated by the second CTM, whereas the CH₄ values from the first CTM will need to be heavily revised to fall within the narrow “trained range” before being input to the NN of the second CTM.

An extreme case of this phenomenon is seen in the CH₄ swap between CAM-Chem and GEOS-Chem (Figure 6a): mixing ratios of CH₄ within GEOS-Chem are prescribed as 1740 ppb throughout the troposphere for the POLMIP simulation. To prevent the extrapolation of the GEOS-Chem NN by using unfamiliar values of CH₄, all incoming CH₄ values must be set to 1740 ppb. The GEOS-Chem NN, therefore, is unable to represent the impact of CH₄ on OH, despite the fact that loss or production of OH (which depends on NO_x) via the oxidation of CH₄ is represented within the chemical mechanism of GEOS-Chem. For this reason, Figure 6a shows no effect of CH₄ on OH and τ_{CH_4} . To obtain scientifically meaningful results, great care must be used in NN analysis to assure the derived functions are interpolations and not extrapolations, due to the highly non-linear behavior of the basis functions. The only alternative for the use of NNs to examine the cause of inter-model difference in modeled OH would be for each group to share the code of their chemical mechanism, which would then allow for the full range of swapped variables to be considered.

Another point to note is that regions in which strong differences in OH are calculated require two necessary conditions: 1) the variables being swapped between the respective NNs must be significantly different at the grid point, and 2) the NN must demonstrate a significant

response of OH due to that variable. It is possible that differences in a swapped variable may be large, yet the response in OH is small due to the weak dependence of OH chemistry on that variable. Therefore, large values of OH column mass differences in Figs. 5, 6, S9, and S10 indicate that the magnitude of the swapped parameter varies significantly between the two CTMs and that this parameter has a considerable impact on the chemistry of OH.

Table 4 lists the effects on τ_{CH_4} of all variable swaps between the GEOS-Chem and CAM-Chem CTMs for July 2008. The variables are listed in order of their impact on τ_{CH_4} . Next, the $\Delta\tau_{\text{CH}_4}$ values due to all inputs are summed ($\Delta\tau_{\text{CH}_4, \text{TOT}}$). It is often the case that the total $\Delta\tau_{\text{CH}_4}$ accounts for the majority of the difference in τ_{CH_4} between the parent CTMs (denoted by τ_{ORIG}). This is true for CAM-Chem and GEOS-Chem: the adjusted τ_{CH_4} for GEOS-Chem, 7.32 years, nearly matches the original CAM-Chem τ_{CH_4} of 7.44 years, while the adjusted CAM-Chem τ_{CH_4} of 7.99 years is close to the original GEOS-Chem τ_{CH_4} of 8.29 years. We attribute the remaining difference between $(\tau_{\text{ORIG}} + \Delta\tau_{\text{CH}_4, \text{TOT}})$ from one model and τ_{ORIG} of the second model to the sum of two terms: variations in the chemical mechanisms of the two models plus differences driven by non-linearities of substituted inputs. This term is referred to as “Mechanism + non-linearities” in Table 4 and as “Mech.+Nonlin.” in subsequent figures.

Table 4 shows that for the July 2008 POLMIP archive of GEOS-Chem and CAM-Chem, variations in the representation of CO by the respective CTMs is the largest single factor driving the 0.85 year difference in τ_{CH_4} . The second most important factor is differences in the respective models’ representation of NO_x . The third factor, and only other important parameter for this model pair, is $J(\text{O}_3 \rightarrow \text{O}(^1\text{D}))$. The magnitude of the difference in τ_{CH_4} due to mechanism plus non-linearities is less than that of the $J(\text{O}_3 \rightarrow \text{O}(^1\text{D}))$ swap.

The quantification of the reasons for the difference in OH (and hence τ_{CH_4}) between GEOS-Chem and CAM-Chem shown in Table 4 provides a roadmap for how to assess the

oxidation capacity of the troposphere within these CTMs. One could, in theory, devise a means to compare fields of CO and $J(\text{O}_3 \rightarrow \text{O}(^1\text{D}))$ within these models to observations and thereby assess the computed fields. However, Table 4 represents just a single model pair, for a particular month. In the next section, we generalize Table 4 to all possible model pairs, for all of the considered months.

3.3 Aggregate Results for All POLMIP CTMs

The large number of comparisons conducted among eight CTMs for nine parameters in each of four months necessitates the aggregation of results to determine the primary drivers of differences in τ_{CH_4} . The overall effect of one variable on the value of τ_{CH_4} within a CTM is assessed by averaging the $\Delta\tau_{\text{CH}_4}$ values due to substitution of that variable from all of the other CTMs. The results of this analysis are shown in **Figure 7** for the average of the four months analyzed here and in **Figure S11** for the four months individually. The points show the mean $\Delta\tau_{\text{CH}_4}$ values, and the error bars represent the standard deviation of the various swaps of the indicated variables. As with Table 4, the difference between the sum of the $\Delta\tau_{\text{CH}_4}$ values for all of the swaps and the gap in τ_{ORIG} of the two parent CTMs is ascribed to chemical mechanism plus non-linearities (Mech.+Nonlin.). The variables are placed in order of decreasing importance, with the exception that Mech.+Nonlin. always appears last, representing its origin as a remainder term. Across all models, for the four months examined (Figure S11) as well as the average of these four months (Figure 7), $J(\text{O}_3 \rightarrow \text{O}(^1\text{D}))$, O_3 , and CO consistently drive the highest mean absolute values of $\Delta\tau_{\text{CH}_4}$. On average, the $\Delta\tau_{\text{CH}_4}$ value resulting from model swaps of $J(\text{O}_3 \rightarrow \text{O}(^1\text{D}))$ is 0.31 years, from O_3 is 0.30 years, and from CO is 0.23 years. Water, NO_x , and CH_4 rank as the fourth through sixth greatest drivers of τ_{CH_4} differences; $J(\text{NO}_2)$ and isoprene occupy the seventh and eighth positions; and temperature accounts for practically none of the difference in τ_{CH_4} .

An unexpected outcome from this analysis is the small effect of changing isoprene, despite the effort being extended by the atmospheric chemistry community to improve the representation of isoprene decomposition products in global models [Crouse et al., 2011; Mao et al., 2013b]. The small role for isoprene likely results from its short lifetime that confines enhancements, relative to background, to the lowest few kilometers above active source regions. While the oxidation of isoprene is of great importance to surface O_3 in, for example, the southeast US [Mao et al., 2013b; Canty et al., 2015; Wolfe et al., 2015], it is less important for τ_{CH_4} because the bulk of CH_4 oxidation occurs over the oceans in the tropics, where OH is highest [Bloss et al., 2005]. For most of this region, differences in mixing ratios of isoprene are too small to appreciably affect globally averaged, tropospheric OH. However, isoprene likely has an indirect effect on remote tropospheric OH that is not accounted for by this method. The reaction of the oxidation products of isoprene with NO_2 leads to the formation of PAN, a reservoir of NO_x capable of being transported long distances [Singh and Salas, 1983]. Thermal decomposition of PAN to release NO_x radicals far from the source subsequently enhances OH secondary production. As a result of the direct role of NO_x in altering OH chemistry in this pathway, the indirect role of isoprene is likely attributed to NO_x differences in this analysis.

Inspection of the aggregated results reveals interesting patterns that provide insight into model behavior. The swaps of $J(O_3 \rightarrow O(^1D))$ reveal that GMI always has a lower mean data point for $\Delta\tau_{CH_4}$ compared to the other models. This suggests that the $J(O_3 \rightarrow O(^1D))$ field native to GMI contributes a positive offset to τ_{CH_4} from this model; i.e., when $J(O_3 \rightarrow O(^1D))$ from other models is substituted into GMI, τ_{CH_4} always drops. Since τ_{CH_4} is proportional to the reciprocal of OH, this implies $J(O_3 \rightarrow O(^1D))$ from GMI is lower than this photolysis frequency in other models. This is confirmed by looking at the fields of $J(O_3 \rightarrow O(^1D))$ at a particular pressure level, 850 hPa, for each model (**Figure 8**).

We also provide plots showing tropospheric O₃ columns from each model (**Figure 9**) to further demonstrate the utility of the NN analysis. Figure 7 shows that GEOS-Chem has the most negative value of $\Delta\tau_{\text{CH}_4}$ for swaps of O₃. This implies that GEOS-Chem has the lowest value of tropospheric O₃, since when O₃ is swapped from all other CTMs into the GEOS-Chem NN, OH consistently rises. The low value of O₃ within GEOS-Chem, relative to the other models, is apparent in Figure 9. While it is possible to compare each of these modeled fields visually or using a statistical method, the neural networking approach provides a means to analyze many variables, including τ_{CH_4} , in a consistent, quantitative, systematic manner.

The Mech.+Nonlin. factor accounts for the largest values of $\Delta\tau_{\text{CH}_4}$ across all months, with a mean absolute value of 0.46 years for the average of the four months (Figure 7). Models that consistently have Mech.+Nonlin. data points that lie close to another CTM (i.e., GMI and GEOS-Chem) are presumed to have very similar chemical mechanisms. Models that exhibit Mech.+Nonlin. data points that consistently differ from the other CTMs, such as TOMCAT, presumably are running a different chemical mechanism than the other models. The NN analysis suggests the chemical mechanism within TOMCAT causes a reduction in τ_{CH_4} of 1.36 years relative to the other seven models and that the mechanism within LMDz-INCA causes an increase in τ_{CH_4} of 0.58 years. As shown in Table 3, TOMCAT exhibits the smallest annual average value of τ_{CH_4} (8.0 years) and LMDz-INCA has the highest value (11.6 years). Our analysis suggests a considerable portion of these two outliers could be due to the chemical mechanism, provided that the primary driver of the Mech.+Nonlin. terms is indeed the mechanism.

The Mech.+Nonlin. term also encompasses effects due to non-linearities either inherent within the chemical mechanism or accrued by asymmetric variable swapping. It is known, for instance, that the production or loss of OH, upon oxidation of CH₄, is a sensitive

function of NO_x [Section 11.3.3 of Jacob, 1999]. The true dependence of OH as a function of CH_4 and NO_x may not be properly represented by summing the individual contributions from swapped CH_4 and swapped NO_x . Also as discussed in Section 2.3, the method we use to prevent NNs from extrapolating outside of the input ranges on which they are trained can result in asymmetry of the swapped variables; the extent to which this occurs can also increase the remainder Mech.+Nonlin. term. By tracking the number of swapped inputs into the NN of a given CTM that invoke extrapolation control, i.e. are adjusted up or down to lie within the trained range of the NN, the TOMCAT model has the 2nd largest percentage of adjusted points (11.2%). The CTM with the largest number of extrapolation-controlled inputs is GEOS-Chem (17.1%); the use of constant mixing ratios of CH_4 is the main reason extrapolation control is invoked in this CTM. Even though CH_4 swaps with GEOS-Chem are consequently asymmetrical, the minimal influence of CH_4 changes on τ_{CH_4} likely explains the near-zero Mech.+Nonlin. term that results for GEOS-Chem. The 3rd highest percentage of extrapolation-controlled points occurs for LMDz-INCA, which has the second lowest Mech.+Nonlin. term. However, as noted above, LMDz-INCA has the highest value for τ_{CH_4} , consistent with the sign and magnitude of the Mech.+Nonlin. term. Overall, the effect of variable swaps that are not exactly equal and opposite does likely play a small role in explaining the Mech.+Nonlin. terms derived from this analysis.

Further work is needed to elucidate the contribution of chemical mechanisms within CTMs to differences in OH and hence τ_{CH_4} . We suggest that, for future model intercomparison projects, each group be asked to run their mechanism in box model mode for prescribed inputs of the nine primary drivers of OH used here, perhaps extracted from a single global model run for a diversity of atmospheric conditions, so that the true variation of OH due to chemical mechanism can be quantified. In the next section, we describe a box

analysis using an external chemical mechanism, not associated with any POLMIP model, to serve as a standard against which all eight CTMs can be evaluated.

3.4 Box model evaluation of CTM chemical mechanisms

We use the DSMACC box model to quantify possible contributions of the chemical mechanisms within individual CTMs to the model differences in $[\text{OH}]^{\text{TROP}}$. Percent differences between the tropospheric OH column mass values calculated by each CTM and the box model, across 4 regions (Figure 4) for the month of April, are shown in **Figure 10**. While the tendency for the box model to predict higher OH mass columns compared to all of the CTMs is apparent, variations in the results indicate differences in the chemical mechanisms between CTMs that may be contributing to the Mech.+Nonlin. term introduced in Section 3.2. The best agreement and low absolute value of the mean percent difference (9%) between TOMCAT and box model OH mass column, compared to the larger absolute value mean percent differences for the other CTMs (~12-22%) suggests that the chemical mechanism within TOMCAT may explain the tendency of OH from this model to be high, compared to other CTMs. This agrees with the large, positive value of the Mech.+Nonlin. term calculated by the TOMCAT NN (Figure 7), which indicates that τ_{CH_4} is low in TOMCAT as a result of its chemical mechanism and non-linearities in the variable swaps. Likewise, LMDz-INCA and C-IFS have the largest absolute values of mean percent difference between CTM and box model OH mass column. The suggestion of low OH resulting from the chemical mechanisms implemented in these two CTMs is in agreement with the NN calculation of the most negative Mech.+Nonlin. $\Delta\tau_{\text{CH}_4}$ values among the eight CTMs evaluated here. The relative ordering of the box model and NN Mech.+Nonlin. results from the remaining CTMs is not perfect; this is likely because the effects of non-linearities in NN variable swaps is not evaluated by the box model approach. However, the agreement of

the box model analysis with the highest and lowest values of $\Delta\tau_{\text{CH}_4}$ attributed to Mech.+Nonlin. by the NN method lends support to our notion that the remainder term is indicative of differences that exist between the eight chemical mechanisms of the POLMIP CTMs.

4 Discussion

We have shown that $J(\text{O}_3 \rightarrow \text{O}(^1\text{D}))$, O_3 , and CO in addition to chemical mechanisms and non-linearities, drive the greatest difference in τ_{CH_4} among the CTMs that participated in POLMIP. Global model representation of fields of tropospheric O_3 and CO as well as the frequency for production of electronically excited $\text{O}(^1\text{D})$ atoms upon photolysis of O_3 , combined with the chemical mechanism that drives the chemistry of OH within these models, are the most important areas to examine to assess why globally averaged, tropospheric OH varies among the eight modeling groups that submitted sufficient output of chemical fields to the POLMIP archive to be used in this study.

The extent of differences in OH due to driving parameters does vary somewhat, depending on which model is being examined. Figure 7 is meant to serve as a guide for how the behavior of a particular CTM differs from the others. For instance, LMDz-INCA has anomalously low OH primarily due to its high CO , low H_2O , and chemical mechanism that tends to underestimate OH , relative to the other POLMIP CTMs. The TOMCAT CTM, on the other hand, exhibits OH higher than the other models in this intercomparison, attributable almost entirely to its chemical mechanism. Likewise, OH in GEOS-Chem is somewhat small due to low concentrations of O_3 and high CO , though offset somewhat by high H_2O . The CAM-Chem CTM has relatively large OH , due to high $J(\text{O}_3 \rightarrow \text{O}(^1\text{D}))$, low CO , and high H_2O , though offset by low local O_3 and NO_x .

It is important to examine whether the factors that we identify as being the primary drivers of OH differences are truly impacting OH concentrations rather than OH concentrations impacting them. CO is the species most likely to be correlated with, but not the cause of, OH variations since its main loss process is reaction with OH. We explore this possibility by comparing $\Delta\tau_{\text{CH}_4}$ values due to CO swaps between CTMs that share similar chemical mechanisms. Across all four examined months, for the model pairings in which the mean $\Delta\tau_{\text{CH}_4}$ attributed to the Mech.+Nonlin. term was less than 0.25 years (29 total pairings), the mean $\Delta\tau_{\text{CH}_4}$ due to differences in CO was 0.05 years higher than the mean $\Delta\tau_{\text{CH}_4}$ due to CO from all model pairings. Likewise, regressing $\Delta\tau_{\text{CH}_4}$ due to CO against $\Delta\tau_{\text{CH}_4}$ due to Mech.+Nonlin. shows a near-complete lack of correlation (for January, $r^2 = 0.00$; April: $r^2 = 0.03$; July: $r^2 = 0.10$; October: $r^2 = 0.03$). If OH differences were responsible for creating variations in model fields of CO, we would expect CTMs that are unbiased with respect to their chemical mechanisms, as compared to each other, to share similar CO burdens and distributions. Since this is not the case, there is some confidence that CO is a driver of OH differences, and the CO variations between CTMs, in turn, must be caused by different implementations of emissions inventories or differences in secondary production from oxidation of VOCs.

We also recognize that these results do not provide clear indication of how to “fix” a particular CTM. The species examined here are interrelated, so a bias in a chemical species such as O_3 could arise due to differences in production from CO, NO_x , and isoprene or in loss by photolysis, indicated by $J(\text{O}_3 \rightarrow \text{O}(^1\text{D}))$, followed by reaction of $\text{O}(^1\text{D})$ with H_2O . For a given model, considering all $\Delta\tau_{\text{CH}_4}$ results by species (Figure 7) in combination helps to elucidate interplay between biases in the various NN inputs. For example, results show that GMI has high O_3 relative to the other CTMs, accompanied by low $J(\text{O}_3 \rightarrow \text{O}(^1\text{D}))$ and high CO. In this case, the low photolysis frequency and high CO concentration are the likely

causes of high O_3 as opposed to fields of NO_x or isoprene, which are, on average, in agreement with the other CTMs. On the other hand, TM5 exhibits high O_3 in combination with high $J(O_3 \rightarrow O(^1D))$, low CO, low CH_4 , and high NO_x . Here, the high concentrations of NO_x are the only viable explanation for high O_3 . Whether the low $J(O_3 \rightarrow O(^1D))$ and high CH_4 in GMI and the high NO_x in TM5 are driven by differences in photolysis scheme, chemical mechanism, emissions, or dynamics is an area for future research. It is interesting to note that other examinations of the POLMIP CTM simulations yield similar results. Though focused on latitudes north of $50^\circ N$, Arnold et al. [2015] showed rank ordering of model biases in O_3 and CO (as compared to data collected during the Arctic Research of the Composition of the Troposphere from Aircraft and Satellites campaign) that are in very good agreement with our results. Similarly, Monks et al. [2015] presented global tropospheric burdens of CO and H_2O that corroborate our findings. Finally, Emmons et al. [2015] demonstrated the same rank ordering between MOZART-4, CAM-Chem, and TOMCAT $J(O_3 \rightarrow O(^1D))$ values as found by the current NN approach, though again limited to the Arctic region. We also stress that all results are relative to other models included in the intercomparison, so this analysis offers no indication of accuracy relative to the actual atmosphere.

This NN method provides a unique and efficient way to diagnose the persistent discrepancy between empirical and model estimates of τ_{CH_4} . The scope of the present analysis, to quantify the factors causing τ_{CH_4} to range from 8.0–11.6 years among the POLMIP CTMs, does not directly address why τ_{CH_4} from global models generally lies below the recent empirical estimate of 11.2 ± 1.3 years given by Prather et al. [2012]. Comparison of each CTM to a common chemical mechanism, the MCM version 3.3.1, indicates how the models perform against a more complete and explicit representation of tropospheric chemistry. As shown above, the OH mass column found using MCM 3.3.1 in a box model

framework, constrained by POLMIP output, tends to exceed the values of OH found by the CTMs (Figure 10). On one hand, this might suggest that the discrepancy for τ_{CH_4} will worsen as a result of our findings. At face value, the box model comparisons show that if the chemical mechanisms within CTMs could be improved to represent tropospheric chemistry as well as MCM 3.3.1, which is a state-of-the-art, detailed chemical mechanism, then CTM OH might be expected to increase, which would lead to a further decrease in τ_{CH_4} . However, the inclusion of additional VOCs and other OH sinks as constraints for the box model driven by MCM 3.3.1, which exist in the real atmosphere and are simulated in many of the POLMIP CTMs, but are not provided as output in the POLMIP archive and thus are not included in the box model analysis, would likely bring the box model into better agreement with OH from the CTMs [e.g., Mao et al., 2009]. Therefore, we would caution against drawing any conclusions about the accuracy of τ_{CH_4} from this model intercomparison. Rather, future applications of this technique to data sets that include measurements of OH, and which utilize a CTM archive that holds the entire suite of modeled VOCs, hold promise for elucidating whether global models are truly overestimating the oxidizing capacity of the troposphere.

Fortunately, a prime opportunity to constrain τ_{CH_4} using observations is currently underway. The NASA Atmospheric Tomography Mission (ATom) field campaign [NASA, 2016] is using the DC-8 aircraft to fly along transects up and down the Pacific and Atlantic Oceans, with a full chemistry payload of instruments. The first scientific question ATom seeks to address is “What are [the] chemical processes that control the short-lived climate forcing agents CH_4 , O_3 , and BC [black carbon] in the atmosphere?”. This venture will be of great utility in testing OH in global models.

Flights of ATom will take place primarily over the oceans. The background atmospheric composition sampled in these regions is likely most important in driving the τ_{CH_4} differences among the models we work with here, since oceans account for the largest surface

area within the band of tropical high OH. A straightforward analysis was performed in which we calculated the sum of the model grid box air mass, as well as the denominator in Eq. 1, over land and over ocean separately. About 75% of the loss of CH₄ due to reaction with OH within the POLMIP CTMs occurs due to grid boxes that reside over ocean. On the other hand, there is a larger variation in OH over land (standard deviation about the mean of 15.1%) within these CTMs than over the ocean (standard deviation of 9.3%). While sampling of OH and related species over land would also provide useful information, it is likely that the larger importance of loss of CH₄ due to reaction with OH over oceans will allow data from ATom to assess and improve the representation of τ_{CH_4} within CTMs.

As noted above, there is widespread recent interest in the influence of isoprene on HO_x (HO_x=OH+HO₂) chemistry, apparent by the number of studies on the topic [e.g. Crouse et al., 2012; Mao et al., 2012; Taraborrelli et al., 2012; Mao et al., 2013b]. However, our primary analysis (Figure 7) suggests that isoprene is not a large factor affecting CTM differences in τ_{CH_4} . To look into this further, we repeated the analysis in the previous paragraph, using an “elevated isoprene” mask rather than a land mask. The mask was determined by flagging model grid points for which the multi-model mean isoprene mixing ratio exceeded 0.05 ppb over land and at pressures greater than 700 hPa. Then, separately for each model, the summed air mass and summed OH terms were determined for the flagged locations. The OH term reveals that 8.2% of tropospheric OH resides in air with elevated isoprene. However, air mass included within elevated-isoprene regimes only accounts for 3.3% of the total tropospheric air mass. These values confirm that isoprene likely has a small role in influencing the difference in τ_{CH_4} among the eight POLMIP CTMs. The short lifetime and localized abundances of isoprene restrict its importance to the regions of biogenic origin.

A final caveat that must be noted is possible co-dependency of the variables that determine primary production of OH: O₃, J(O₃→O(¹D)), and H₂O. These three parameters

could vary in a manner that could complicate the analysis. For example, if larger photolysis frequency (relative to other models) happens to lead to greater loss of local O_3 , it is possible that the effect of these two factors cancel and primary production of OH remains unaffected.

A cursory evaluation of this effect has been conducted by regressing values of $\Delta\tau_{CH_4}$ due to variable swaps of O_3 against $\Delta\tau_{CH_4}$ found from variable swaps of $J(O_3 \rightarrow O(^1D))$ (**Figure S12**).

The anticorrelation of these two factors among the eight CTMs is weak ($r^2 = 0.06$), suggesting that canceling effects of O_3 and $J(O_3 \rightarrow O(^1D))$ on primary production of OH are not identifiable in this analysis. Therefore, we attribute significance to our NN results that indicate O_3 and/or $J(O_3 \rightarrow O(^1D))$ are influencing large inter-model differences in OH.

Further development of this technique is encouraged to best reproduce model OH chemistry through NN training. Persistent regions of disagreement between a NN and its CTM, such as over certain continental regions, likely indicates the exclusion of a parameter in the NN that is influencing OH chemistry in the CTM. While a strength of this technique is the ability to perform the analysis with a minimal amount of model output, it is probably worthwhile to explore the impact of inclusion of other species like HCHO, other VOCs (e.g. ethane, propane, acetone, acetaldehyde), lightning NO_x , and aerosol surface area density. Alternative inputs, such as OH chemical production and loss terms, might also be considered, with applications more directed toward studying the chemical mechanisms that drive OH. Additionally, while the NN architectures used here were thoroughly vetted in terms of minimizing errors and maintaining reasonable computation times, it is likely that more powerful computers could efficiently train neural networks with more nodes, more hidden layers, or both to further improve their accuracy in modeling OH chemistry. While the process of creating an NN is somewhat computationally intensive, once established, that NN can be “re-run” with alternative inputs near instantly. As a result, this approach has a significant time saving benefit over re-running an entire CTM.

5 Conclusions

Neural networks were used to quantify the factors driving differences in tropospheric OH and the methane lifetime, τ_{CH_4} , among the CTMs that participated in POLMIP. Annual mean values of τ_{CH_4} ranged from 8.0 years for the TOMCAT model to 11.6 years for the LMDz-INCA model. NNs were trained to reproduce monthly mean 3-D fields of OH mixing ratios for each CTM using inputs of H_2O , O_3 , NO_x , CO, CH_4 , isoprene, $J(\text{O}_3 \rightarrow \text{O}(^1\text{D}))$, $J(\text{NO}_2)$, pressure, latitude, and temperature. Trained NNs were then used to estimate the effect on OH of replacing individual input fields with fields from another CTM. Values of $\Delta\tau_{\text{CH}_4}$ indicate to what degree a given input is influencing model differences in τ_{CH_4} . Overall, $J(\text{O}_3 \rightarrow \text{O}(^1\text{D}))$, O_3 , and CO account for the largest variation of $\Delta\tau_{\text{CH}_4}$ among the eight CTMs, along with indirectly evaluated differences in model chemical mechanisms and nonlinearities in the variable swaps. On an annual basis and across all model pairings, $J(\text{O}_3 \rightarrow \text{O}(^1\text{D}))$ accounted for an average model $\Delta\tau_{\text{CH}_4}$ of 0.31 years, O_3 accounted for that of 0.30 years, and CO accounted for that of 0.23 years. While these results are representative of average $\Delta\tau_{\text{CH}_4}$ values across all model pairings, it is useful to examine individual model results to understand which fields should be targeted for further examination for any one CTM.

Box modeling was performed to examine the veracity of CTM mechanistic differences suggested by the NN analysis. Those models for which the “Mech.+Nonlin.” $\Delta\tau_{\text{CH}_4}$ term is highest (TOMCAT with $\Delta\tau_{\text{CH}_4} = +1.36$ years) and lowest (C-IFS with $\Delta\tau_{\text{CH}_4} = -0.74$ years and LMDz-INCA with $\Delta\tau_{\text{CH}_4} = -0.58$ years) have the highest and lowest tropospheric OH mass column differences (CTM – Box Model), respectively, compared with columns calculated using the box model. This supports our method of attributing the remainder τ_{CH_4} difference between models not accounted for by the total $\Delta\tau_{\text{CH}_4}$ from each NN

input to mechanistic differences. A more in-depth box modeling study using higher frequency model output is required to identify the precise nature of these suggested mechanistic differences.

The neural network method described here offers a computationally efficient way to approximate the OH chemistry implemented within various CTMs, without access to the detailed chemical mechanism. Output requirements for the archive are not burdensome and multi-model intercomparisons can be conducted in a straightforward manner, provided all modeling groups archive the same chemical fields. Here we showed that this analysis is possible with only monthly mean output of the fields: p, T, latitude, H₂O, O₃, NO_x, CO, CH₄, isoprene, J(O₃→O(¹D))), J(NO₂), and OH. However, including indicators of cloud coverage, lightning NO_x, aerosols, additional VOCs, and fast radical chemistry would likely improve NN performance and provide useful information regarding the cause of the differences in OH precursors and sinks. As such, we suggest that cloud fraction, NO_x produced by lightning, total aerosol surface area density, and the species HCHO, CH₃CHO, acetone, propane, ethane, HO₂, and any applicable RO₂ radicals also be included in future archives used to conduct similar analyses. In addition, higher temporal frequency of model output (i.e., at least hourly for certain, select days) would allow for analysis of fast OH chemistry that depends strongly on solar illumination. Trained neural networks can perhaps be further developed for future evaluations of coupled climate chemistry models, as well as for comparisons of model output to global measurements of OH and related chemical compounds, such as the data that will be provided by the ongoing NASA ATom campaign. We demonstrate here that NNs are capable of accurately reproducing 3-D fields of OH from a global CTM using minimal model output. Application of the neural network tool to global observational data sets, such as ATom, has the capacity to serve as a means to quantitatively evaluate the accuracy of the CH₄ lifetime in global models.

It is imperative that the large spread in CH₄ lifetime values between models simulating present-day conditions be understood and improved to ensure that forecasts of future climate, which depends strongly on the CH₄ abundance, are as accurate as possible. The present discrepancy between multi-model means and empirically derived estimates of CH₄ lifetime call into question whether projections of the future oxidizing capacity of the troposphere, which can only be obtained using models, provide a useful guide for what might truly happen. Neural networks, which offer a means to quantify the cause of differences in the CH₄ lifetime found by various models, could be an important tool for addressing this deficiency in our understanding of OH on the global scale.

6 Acknowledgments

We thank the three anonymous reviewers for providing constructive feedback that led to improvement of this manuscript. We also thank Bryan Duncan for helpful discussions concerning the development of this method. The POLMIP model simulations are available upon request to the authors (julie.m.nicely@nasa.gov). Work conducted at the University of Maryland was supported, in part, by the NASA Modeling and Analysis Program. JMN was also supported by an appointment to the NASA Postdoctoral Program at the NASA Goddard Space Flight Center, administered by Universities Space Research Association under contract with NASA. The National Center for Atmospheric Research is funded by the National Science Foundation. VH acknowledges funding by the European Union's Seventh Framework Programme (FP7) for MACC III under grant agreement no. 283576.

7 References

- Allison, T. C. (2015), Application of an Artificial Neural Network to the Prediction of OH Radical Reaction Rate Constants for Evaluating Global Warming Potential, *J. Phys. Chem. B*, doi:10.1021/acs.jpcc.5b09558.
- Arnold, S. R., et al. (2015), Biomass burning influence on high-latitude tropospheric ozone and reactive nitrogen in summer 2008: a multi-model analysis based on POLMIP simulations, *Atmos. Chem. Phys.*, 15, 6047-6068, doi:10.5194/acp-15-6047-2015.
- Beale, M. H., M. T. Hagan, and H. B. Demuth (2013), *Neural Network Toolbox User's Guide*, The MathWorks, Inc., Natick, MA, available at <https://www.mathworks.com/help/nnet/>.
- Bey, I., D. J. Jacob, R. M. Yantosca, J. A. Logan, B. D. Field, A. M. Fiore, Q. Li, H. Y. Liu, L. J. Mickley, and M. G. Schultz (2001), Global modeling of tropospheric chemistry with assimilated meteorology: Model description and evaluation, *J. Geophys. Res.*, 106, 23,073–23,095, doi:10.1029/2001JD000807.
- Bloss, W. J., M. J. Evans, J. D. Lee, R. Sommariva, D. E. Heard, and M. J. Pilling (2005), The oxidative capacity of the troposphere: Coupling of field measurements of OH and a global chemistry transport model, *Faraday Discuss.*, 130, 425-436, doi:10.1039/B419090D.
- Canty, T. P., L. Hembeck, T. P. Vinciguerra, D. C. Anderson, D. L. Goldberg, S. F. Carpenter, D. J. Allen, C. P. Loughner, R. J. Salawitch, and R. R. Dickerson (2015), Ozone and NO_x chemistry in the eastern US: evaluation of CMAQ/CB05 with satellite (OMI) data, *Atmos. Chem. Phys.*, 15(19), 10965-10982, doi:10.5194/acp-15-10965-2015.
- Chipperfield, M. P. (2006), New version of the TOMCAT/SLIMCAT off-line chemical transport model: Intercomparison of stratospheric tracer experiments, *Q. J. R. Meteorol. Soc.*, 132, 1179–1203, doi:10.1256/qj.05.51.
- Comrie, A. C. (1997), Comparing Neural Networks and Regression Models for Ozone Forecasting, *J. Air Waste Manage.*, 47(6), 653-663, doi:10.1080/10473289.1997.10463925.
- Crouse, J. D., F. Paulot, H. G. Kjaergaard, and P. O. Wennberg (2011), Peroxy radical isomerization in the oxidation of isoprene, *Phys. Chem. Chem. Phys.*, 13(30), 13607-13613, doi:10.1039/c1cp21330j.
- Crouse, J. D., H. C. Knap, K. B. Ornsø, S. Jørgensen, F. Paulot, H. G. Kjaergaard, and P. O. Wennberg (2012), Atmospheric Fate of Methacrolein. 1. Peroxy Radical Isomerization Following Addition of OH and O₂, *J. Phys. Chem. A*, 116(24), 5756-5762, doi:10.1021/jp211560u.

- Dee, D. P., et al. (2011), The ERA-Interim reanalysis: configuration and performance of the data assimilation system, *Q. J. Roy. Meteorol. Soc.*, 137, 553-597, doi:10.1002/qj.828.
- Duncan, B., D. Portman, I. Bey, and C. Spivakovsky (2000), Parameterization of OH for efficient computation in chemical tracer models, *J. Geophys. Res. Atmos.*, 105(D10), 12259-12262, doi:10.1029/1999jd901141.
- Duncan, B. N., S. E. Strahan, Y. Yoshida, S. D. Steenrod, and N. Livesey (2007), Model study of the cross-tropopause transport of biomass burning pollution, *Atmos. Chem. Phys.*, 7, 3713–3736, doi:10.5194/acp-7-3713-2007.
- Emmerson, K. M., and M. J. Evans (2009), Comparison of tropospheric gas-phase chemistry schemes for use within global models, *Atmos. Chem. Phys.*, 9(5), 1831-1845, doi:10.5194/acp-9-1831-2009.
- Emmons, L. K., et al. (2010), Description and evaluation of the Model for Ozone and Related chemical Tracers, version 4 (MOZART-4), *Geosci. Model Dev.*, 3, 43–67, doi:10.5194/gmd-3-43-2010.
- Emmons, L. K., et al. (2015), The POLARCAT Model Intercomparison Project (POLMIP): overview and evaluation with observations, *Atmos. Chem. Phys.*, 15(12), 6721-6744, doi:10.5194/acp-15-6721-2015.
- Fiore, A. M., et al. (2009), Multimodel estimates of intercontinental source-receptor relationships for ozone pollution, *J. Geophys. Res. Atmos.*, 114, 21, doi:10.1029/2008jd010816.
- Flemming, J., et al. (2015), Tropospheric chemistry in the Integrated Forecasting System of ECMWF, *Geosci. Model Dev.*, 8, 975–1003, doi:10.5194/gmd-8-975-2015.
- Gardner, M. W., and S. R. Dorling (1998), Artificial neural networks (the multilayer perceptron) - A review of applications in the atmospheric sciences, *Atmos. Environ.*, 32(14-15), 2627-2636, doi:10.1016/s1352-2310(97)00447-0.
- Gramatica, P., V. Consonni, and R. Todeschini (1999), QSAR Study on the Tropospheric Degradation of Organic Compounds, *Chemosphere*, 38(6), 1371–1378, doi:10.1016/S0045-6535(98)00539-6.
- Hauglustaine, D. A., F. Hourdin, L. Jourdain, M.-A. Filiberti, S. Walters, J.-F. Lamarque, and E. A. Holland (2004), Interactive chemistry in the Laboratoire de Météorologie Dynamique general circulation model: Description and background tropospheric chemistry evaluation, *J. Geophys. Res.*, 109, D04314, doi:10.1029/2003JD003957.
- Heaton, J. (2011), Introduction to the math of neural networks, edited, Heaton Research, Inc., St. Louis.

- Hourdin, F., et al. (2006), The LMDZ4 general circulation model: Climate performance and sensitivity to parametrized physics with emphasis on tropical convection, *Clim. Dynam.*, 27, 787–813, doi:10.1007/s00382-006-0158-0.
- Huijnen, V., et al. (2010), The global chemistry transport model TM5: Description and evaluation of the tropospheric chemistry version 3.0, *Geosci. Model Dev.*, 3, 445–473, doi:10.5194/gmd-3-445-2010.
- Intergovernmental Panel on Climate Change (IPCC) (2001), *Climate Change 2001: The Scientific Basis*, in Contribution of Working Group I to the Third Assessment Report of the Intergovernmental Panel on Climate Change, 881 pp., Cambridge Univ. Press, Cambridge, U. K., and New York.
- Intergovernmental Panel on Climate Change (IPCC) (2013), *Climate Change 2013: The Physical Science Basis*, in Contribution of Working Group I to the Fifth Assessment Report of the Intergovernmental Panel on Climate Change, 1535 pp., Cambridge Univ. Press, Cambridge, U. K., and New York.
- Jacob, D. J. (1999), *Introduction to Atmospheric Chemistry*, Princeton Univ. Press, Princeton, N.J.
- Jain, A. K., J. C. Mao, and K. M. Mohiuddin (1996), Artificial neural networks: A tutorial, *Computer*, 29(3), 31-44, doi:10.1109/2.485891.
- Jenkin, M. E., S. M. Saunders, and M. J. Pilling (1997), The tropospheric degradation of volatile organic compounds: A protocol for mechanism development, *Atmos. Environ.*, 31(1), 81-104, doi:10.1016/s1352-2310(96)00105-7.
- Jenkin, M. E., J. C. Young, and A. R. Rickard (2015), The MCM v3.3.1 degradation scheme for isoprene, *Atmos. Chem. Phys.*, 15, 11433-11459, doi:10.5194/acp-15-11433-2015.
- Krol, M., and J. Lelieveld (2003), Can the variability in tropospheric OH be deduced from measurements of 1,1,1-trichloroethane (methyl chloroform)?, *J. Geophys. Res.*, 108(D3), 4125, doi:10.1029/2002JD002423.
- Lamarque, J.-F., et al. (2012), CAM-chem: Description and evaluation of interactive atmospheric chemistry in the Community Earth System Model, *Geosci. Model Dev.*, 5(2), 369–411, doi:10.5194/gmd-5-369-2012.
- Lary, D. J., L. A. Remer, D. MacNeill, B. Roscoe, and S. Paradise (2009), Machine Learning and Bias Correction of MODIS Aerosol Optical Depth, *Ieee Geoscience and Remote Sensing Letters*, 6(4), 694-698, doi:10.1109/lgrs.2009.2023605.
- Law, K., et al. (2014), Arctic Air Pollution: New Insights From POLARCAT-IPY, *Bull. Amer. Meteor. Soc.*, 95(12), 1873-1895, doi:10.1175/BAMS-D-13-00017.1.

- Lee, L. A., K. S. Carslaw, K. J. Pringle, and G. W. Mann (2012), Mapping the uncertainty in global CCN using emulation, *Atmos. Chem. Phys.*, 12, 9739-9751, doi:10.5194/acp-12-9739-2012.
- Lee, L. A., C. L. Reddington, and K. S. Carslaw (2016), On the relationship between aerosol model uncertainty and radiative forcing uncertainty, *P. Natl. Acad. Sci. USA*, 113(21), 5820-5827, doi:10.1073/pnas.1507050113.
- Lelieveld, J., S. Gromov, A. Pozzer, and D. Taraborrelli (2016), Global tropospheric hydroxyl distribution, budget and reactivity, *Atmos. Chem. Phys.*, 16, 12477-12493, doi:10.5194/acp-16-12477-2016.
- Levy, H. (1971), Normal atmosphere: large radical and formaldehyde concentrations predicted, *Science*, 173(3992), 141-143, doi: 10.1126/science.173.3992.141.
- Mao, J., et al. (2009), Airborne measurement of OH reactivity during INTEX-B, *Atmos. Chem. Phys.*, 9, 163-173, doi:10.5194/acp-9-163-2009.
- Mao, J., et al. (2010), Chemistry of hydrogen oxide radicals (HOx) in the Arctic troposphere in spring, *Atmos. Chem. Phys.*, 10(13), 5823-5838, doi:10.5194/acp-10-5823-2010.
- Mao, J., et al. (2012), Insights into hydroxyl measurements and atmospheric oxidation in a California forest, *Atmos. Chem. Phys.*, 12(17), 8009-8020, doi:10.5194/acp-12-8009-2012.
- Mao, J., S. Fan, D. J. Jacob, and K. R. Travis (2013a), Radical loss in the atmosphere from Cu-Fe redox coupling in aerosols, *Atmos. Chem. Phys.*, 13, 509-519, doi: 10.5194/acp-13-509-2013.
- Mao, J., F. Paulot, D. J. Jacob, R. C. Cohen, J. D. Crouse, P. O. Wennberg, C. A. Keller, R. C. Hudman, M. P. Barkley, and L. W. Horowitz (2013b), Ozone and organic nitrates over the eastern United States: Sensitivity to isoprene chemistry, *J. Geophys. Res. Atmos.*, 118(19), 11256-11268, doi:10.1002/jgrd.50817.
- Molod, A., L. Takacs, M. Suarez, J. Bacmeister, I-S. Song, and A. Eichmann (2012), The GEOS-5 atmospheric general circulation model: mean climate and development from MERRA to Fortuna, NASA, Goddard Space Flight Center, Greenbelt, MD.
- Monks, S. A., et al. (2015), Multi-model study of chemical and physical controls on transport of anthropogenic and biomass burning pollution to the Arctic, *Atmos. Chem. Phys.*, 15, 3575-3603, doi:10.5194/acp-15-3575-2015.
- Monks, S.A., et al. (2016), The TOMCAT global chemical transport model: Description of chemical mechanism and model evaluation, *Geophys. Mod. Dev. Discuss.*, doi:10.5194/gmd-2016-212.

- Murray, L. T., J. A. Logan, and D. J. Jacob (2013), Interannual variability in tropical tropospheric ozone and OH: The role of lightning, *J. Geophys. Res. Atmos.*, 118, 11,468–11,480, doi:10.1002/jgrd.50857.
- Naik, V., et al. (2013), Preindustrial to present-day changes in tropospheric hydroxyl radical and methane lifetime from the Atmospheric Chemistry and Climate Model Intercomparison Project (ACCMIP), *Atmos. Chem. Phys.*, 13(10), 5277-5298, doi:10.5194/acp-13-5277-2013.
- NASA (2016), Atmospheric Tomography Mission website, edited, NASA Earth Science Project Office, available at <https://espo.nasa.gov/home/atom>
- Nicely, J., et al. (2016), An observationally constrained evaluation of the oxidative capacity in the tropical western Pacific troposphere, *J. Geophys. Res. Atmos.*, 121, 7461–7488, doi:10.1002/2016JD025067.
- Pan, L. L., W. J. Randel, B. L. Gary, M. J. Mahoney, and E. J. Hintsala (2004), Definitions and sharpness of the extratropical tropopause: A trace gas perspective, *J. Geophys. Res. Atmos.*, 109(D23), 11, doi:10.1029/2004jd004982.
- Patra, P. K., et al. (2014), Observational evidence for interhemispheric hydroxyl-radical parity, *Nature*, 513, 219–223, doi:10.1038/nature13721.
- Prather, M., et al. (2001), Atmospheric chemistry and greenhouse gases, in *Climate Change 2001: The Scientific Basis. Contribution of Working Group I to the Third Assessment Report of the Intergovernmental Panel on Climate Change*, edited by J. T. Houghton et al., edited, pp. 239-287, Cambridge Univ. Press, Cambridge, U.K.
- Prather, M. J., C. D. Holmes, and J. Hsu (2012), Reactive greenhouse gas scenarios: Systematic exploration of uncertainties and the role of atmospheric chemistry, *Geophys. Res. Lett.*, 39, 5, doi:10.1029/2012gl051440.
- Prinn, R. G., et al. (2005), Evidence for variability of atmospheric hydroxyl radicals over the past quarter century, *Geophys. Res. Lett.*, 32(7), 4, doi:10.1029/2004gl022228.
- Rigby, M., et al. (2013), Re-evaluation of the lifetimes of the major CFCs and CH₃CCl₃ using atmospheric trends, *Atmos. Chem. Phys.*, 13, 2691-2702, doi:10.5194/acp-13-2691-2013.
- Rohrer, F. and H. Berresheim (2006), Strong correlation between levels of tropospheric hydroxyl radicals and solar ultraviolet radiation, *Nature*, 442, 184-187, doi:10.1038/nature04924.
- Saunders, S. M., M. E. Jenkin, R. G. Derwent, and M. J. Pilling (2003), Protocol for the development of the Master Chemical Mechanism, MCM v3 (Part A): tropospheric degradation of non-aromatic volatile organic compounds, *Atmos. Chem. Phys.*, 3(1), 161-180, doi:10.5194/acp-3-161-2003.

- Shindell, D. T., et al. (2006), Multimodel simulations of carbon monoxide: Comparison with observations and projected near-future changes, *J. Geophys. Res. Atmos.*, 111(D19), 24, doi:10.1029/2006jd007100.
- Singh, H. B., and L. J. Salas (1983), Peroxyacetyl nitrate in the free troposphere, *Nature*, 302, 326-328, doi:10.1038/302326a0.
- Spivakovsky, C. M., S. C. Wofsy, and M. J. Prather (1990), A numerical method for parameterization of atmospheric chemistry: computation of tropospheric OH, *J. Geophys. Res.*, 95(D11), 18433-18439, doi:10.1029/JD095iD11p18433.
- Strahan, S. E., B. N. Duncan, and P. Hoor (2007), Observationally derived transport diagnostics for the lowermost stratosphere and their application to the GMI chemistry and transport model, *Atmos. Chem. Phys.*, 7, 2435–2445, doi:10.5194/acp-7-2435-2007.
- Stratospheric Processes and their Role in Climate (SPARC) (2013), SPARC Report on Lifetimes of Stratospheric Ozone-Depleting Substances, in Their Replacements, and Related Species, SPARC Rep. 6, WCRP-15/2013, edited by M. K. W. Ko et al. [Available at www.sparc-climate.org/publications/sparc-reports/.]
- Strode, S. A., B. N. Duncan, E. A. Yegorova, J. Kouatchou, J. R. Ziemke, and A. R. Douglass (2015), Implications of carbon monoxide bias for methane lifetime and atmospheric composition in chemistry climate models, *Atmos. Chem. Phys.*, 15(20), 11,789–11,805, doi:10.5194/acp-15-11789-2015.
- Taraborrelli, D., M. G. Lawrence, J. N. Crowley, T. J. Dillon, S. Gromov, C. B. M. Gross, L. Vereecken, and J. Lelieveld (2012), Hydroxyl radical buffered by isoprene oxidation over tropical forests, *Nature Geoscience*, 5(3), 190-193, doi:10.1038/ngeo1405.
- Tilmes, S., et al. (2015), Description and evaluation of tropospheric chemistry and aerosols in the Community Earth System Model (CESM1.2), *Geosci. Model Dev.*, 8(5), 1395–1426, doi:10.5194/gmd-8-1395-2015.
- Urata, S., A. Takada, T. Uchimaru, A. K. Chandra, and A. Sekiya (2002), Artificial Neural Network Study for the Estimation of the C–H Bond Dissociation Energies, *J. Fluorine Chem.*, 116, 163–171, doi:10.1016/S0022-1139(02)00128-8.
- Urata, S., A. Takada, T. Uchimaru, and A. K. Chandra (2003), Rate Constants Estimation for the Reaction of Hydrofluorocarbons and Hydrofluoroethers with OH Radicals, *Chem. Phys. Lett.*, 368, 215–233, doi:10.1016/S0009-2614(02)01718-9.
- Voulgarakis, A., O. Wild, N. H. Savage, G. D. Carver, and J. A. Pyle (2009), Clouds, photolysis and regional tropospheric ozone budgets, *Atmos. Chem. Phys.*, 9, 8235-8246, doi:10.5194/acp-9-8235-2009.

Voulgarakis, A., et al. (2013), Analysis of present day and future OH and methane lifetime in the ACCMIP simulations, *Atmos. Chem. Phys.*, 13(5), 2563-2587, doi:10.5194/acp-13-2563-2013.

Wennberg, P. O., S. Peacock, J. T. Randerson, and R. Bleck (2004), Recent changes in the air-sea gas exchange of methyl chloroform, *Geophys. Res. Lett.*, 31, L16112, doi:10.1029/2004GL020476.

Williams, J. E., P. F. J. van Velthoven, and C. A. M. Brenninkmeijer (2013), Quantifying the uncertainty in simulating global tropospheric composition due to the variability in global emission estimates of Biogenic Volatile Organic Compounds, *Atmos. Chem. Phys.*, 13, 2857–2891, doi:10.5194/acp-13-2857-2013.

Wolfe, G. M., et al. (2015), Quantifying sources and sinks of reactive gases in the lower atmosphere using airborne flux observations, *Geophys. Res. Lett.*, 42(19), 8231-8240, doi:10.1002/2015gl065839.

Accepted Article

Table 1. Estimates of CH₄ lifetime due to removal by OH from recent literature and this study

Method	τ_{CH_4} due to OH	Source
Best estimate from CH ₃ CCl ₃ inversion; range from OxComp CTM evaluation	9.6 (6.5-13.8) ^a	IPCC TAR, 2001
CH ₃ CCl ₃ inversion	10.2 (9.5-11.1) ^b	Prinn et al., 2005
CH ₃ CCl ₃ inversion	11.2 (9.9-12.5) ^b	Prather et al., 2012
CH ₃ CCl ₃ inversion	10.5 (8.0-15.1) ^c	SPARC, 2013; Rigby et al., 2013
CTM model intercomparison (26 models)	9.72 (6.91-15.05) ^a (8.02-11.42) ^b	Shindell et al., 2006
CTM model intercomparison (12 models)	10.19 (6.19-12.50) ^a (8.47-11.91) ^b	Fiore et al., 2009
Chemistry-Climate Model (CCM) intercomparison, ACCMIP (16 models)	9.7 (7.1-14.0) ^a (8.2-11.2) ^b	Naik et al., 2013; Voulgarakis et al., 2013
CCM intercomparison (5 models)	8.9 (7.5-10.3) ^b	SPARC, 2013
CTM model intercomparison (8 models)	9.3 (8.0-11.6) ^a (8.2-10.3) ^b	POLMIP/This study, 2017

^aFull range of values provided.^b1 σ uncertainty provided^c2 σ uncertainty provided

Table 2. Chemical Transport Model simulations from the POLARCAT Model Intercomparison Project used in this study

POLMIP CTM	Resolution	Institution	Reference
CAM-Chem	1.875° × 2.5° 56 levels	National Center for Atmospheric Research, USA	Lamarque et al., 2012; Tilmes et al., 2015
C-IFS	1.125° × 1.125° 60 levels	European Centre for Medium-Range Weather Forecasts, UK	Flemming et al., 2015
GEOS-Chem	2.0° × 2.5° 47 levels	Harvard U., USA	Bey et al., 2001; Mao et al., 2010
GMI	2.0° × 2.5° 72 levels	NASA Goddard Space Flight Center, USA	Duncan et al., 2007; Strahan et al., 2007
LMDz-INCA	1.875° × 3.75° 39 levels	Laboratoire de Météorologie Dynamique, France	Hauglustaine et al., 2004; Hourdin et al., 2006
MOZART-4	1.875° × 2.5° 56 levels	National Center for Atmospheric Research, USA	Emmons et al., 2010
TM5	2.0° × 3.0° 60 levels	Royal Netherlands Meteorological Institute, Netherlands	Huijnen et al., 2010; Williams et al., 2013
TOMCAT	2.81° × 2.81° 31 levels	U. of Leeds, UK	Chipperfield, 2006; Monks et al., 2016

Table 4. Budgeting of τ_{CH_4} between GEOS-Chem and CAM-Chem for July

		GEOS-Chem	CAM-Chem
$\tau_{\text{CH}_4, \text{ORIG}}^{\text{a}}$ (years)		8.29	7.44
$\Delta\tau_{\text{CH}_4, \text{TOT}}^{\text{b}}$	CO	-0.75	+0.47
	NO _x	+0.36	-0.30
	J(O ₃ → O(¹ D))	-0.36	+0.30
	J(NO ₂)	+0.12	+0.06
	CH ₄	0.00	-0.14
	Isoprene	-0.02	+0.09
	POLMIP CTM	-0.06	+0.04
	H ₂ O	0.06	0.00
	O ₃	-0.02	+0.03
	Temp	0.00	0.00
$\Delta\tau_{\text{CH}_4, \text{TOT}}^{\text{c}}$		9.3	+0.55
$\tau_{\text{CH}_4, \text{ORIG}}^{\text{b}}$		11.6	7.99
Mechanism non-linearities ^d		9.0	+0.12

^a $\tau_{\text{CH}_4, \text{ORIG}}$ represents value of τ_{CH_4} evaluated directly from the CTM

^b $\Delta\tau_{\text{CH}_4}$ calculated from output of NN when noted variable is substituted using values from the other CTM

^c Sum of all $\Delta\tau_{\text{CH}_4}$ values calculated for each input substitution

^d “Remainder” of original τ_{CH_4} difference not accounted for by NN substitutions; calculated as $\tau_{\text{CH}_4, \text{ORIG}}(\text{CTM A}) - [\tau_{\text{CH}_4, \text{ORIG}}(\text{CTM B}) + \Delta\tau_{\text{CH}_4, \text{TOT}}(\text{CTM B})]$

Table 3. Annual Average CH₄ lifetime due to loss by the eight CTMs included in this study

CTM	Annual Average τ_{CH_4} (years)
CAM-Chem	8.6
C-IFS	9.3
GEOS-Chem	9.6
GMI-GEOS5	9.3
HMZ-INGA	11.6
MOZART	9.0
TMS	8.8
TOMCAT	8.0

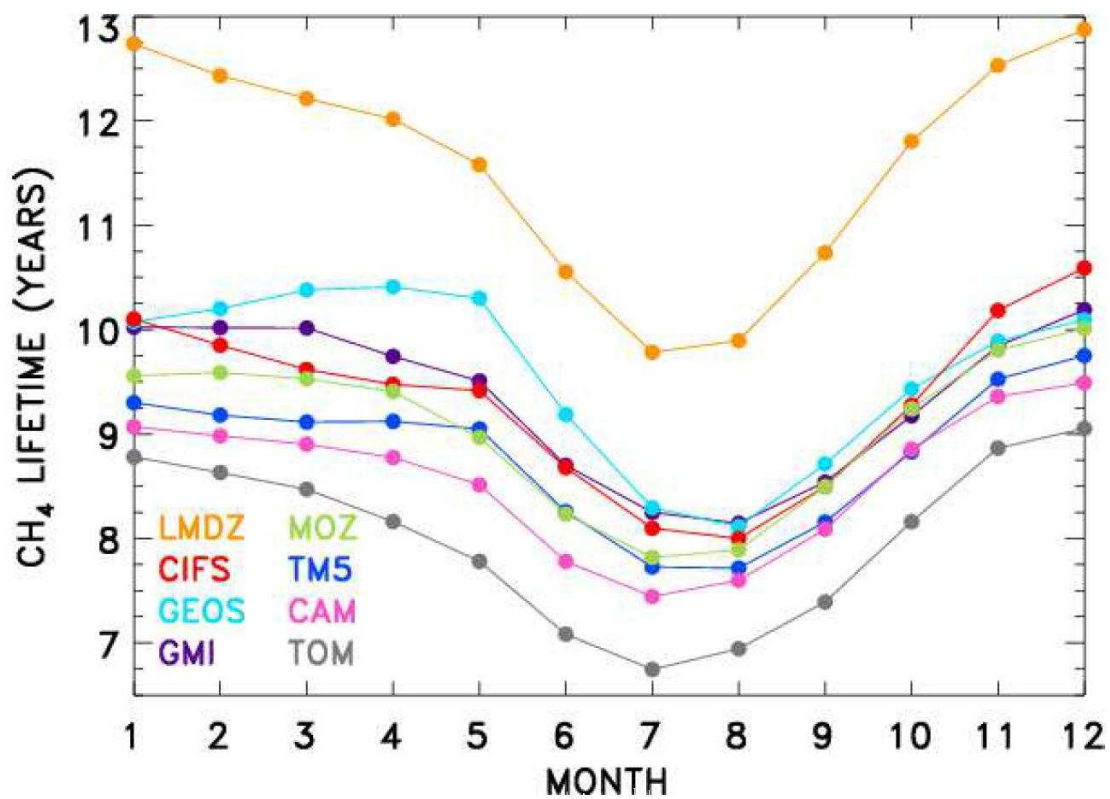


Figure 1. Tropospheric CH₄ lifetime by month calculated for each POLMIP CTM included in this analysis. CAM indicates CAM-Chem version 4. Values of τ_{CH_4} are calculated as the tropospheric CH₄ burden divided by the CH₄ loss rate due to reaction with OH from monthly mean output. Labels are listed in descending order of January lifetime values.

Accepted

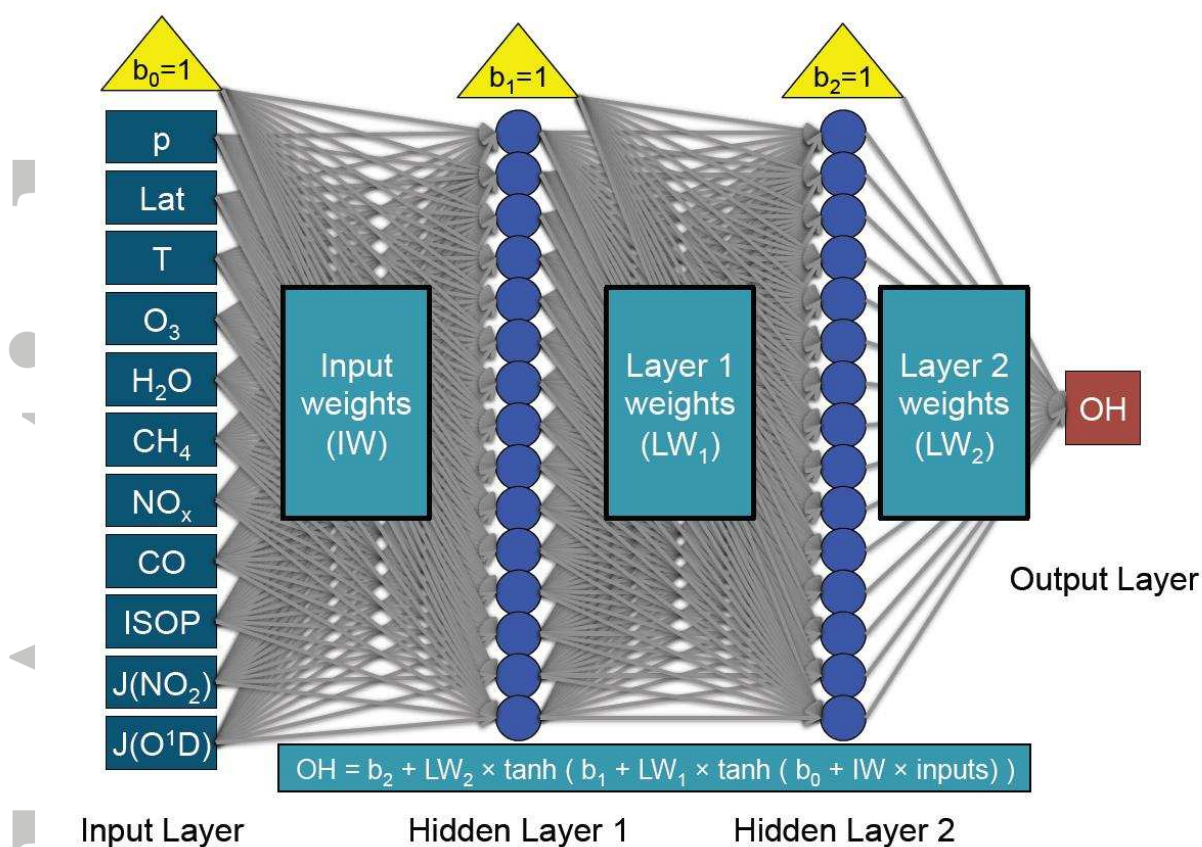


Figure 2. Architecture of the NNs used in the present study for all CTMs except GEOS-Chem, C-IFS, and TOMCAT. The NN consists of two hidden layers, each containing 15 nodes (represented by blue circles). The NNs for GEOS-Chem, C-IFS, and TOMCAT contain 30 nodes per hidden layer instead of 15. The 11 input parameters are listed on the left (dark green boxes). Values are input as unitless mixing ratios for all chemical species except CH₄, units of s⁻¹ for photolysis frequencies J(O¹D) and J(NO₂), K for temperature, and hPa for pressure. For CH₄, values are scaled relative to the maximum CH₄ within the troposphere for a given model such that the input value represents a ratio between 0 and 1. Hyperbolic tangent activation functions are performed on the linear combination of the inputs multiplied by their input weights (represented by grey arrows) at each node in Hidden Layer 1; those values are fed forward with additional weightings (Layer 1 weights) to the Hidden Layer 2, where a second series of activation functions are performed. Output from Hidden Layer 2 is weighted once more (Layer 2 weights) and linearly combined to give a single OH mixing ratio for a given latitude, longitude, and pressure level.

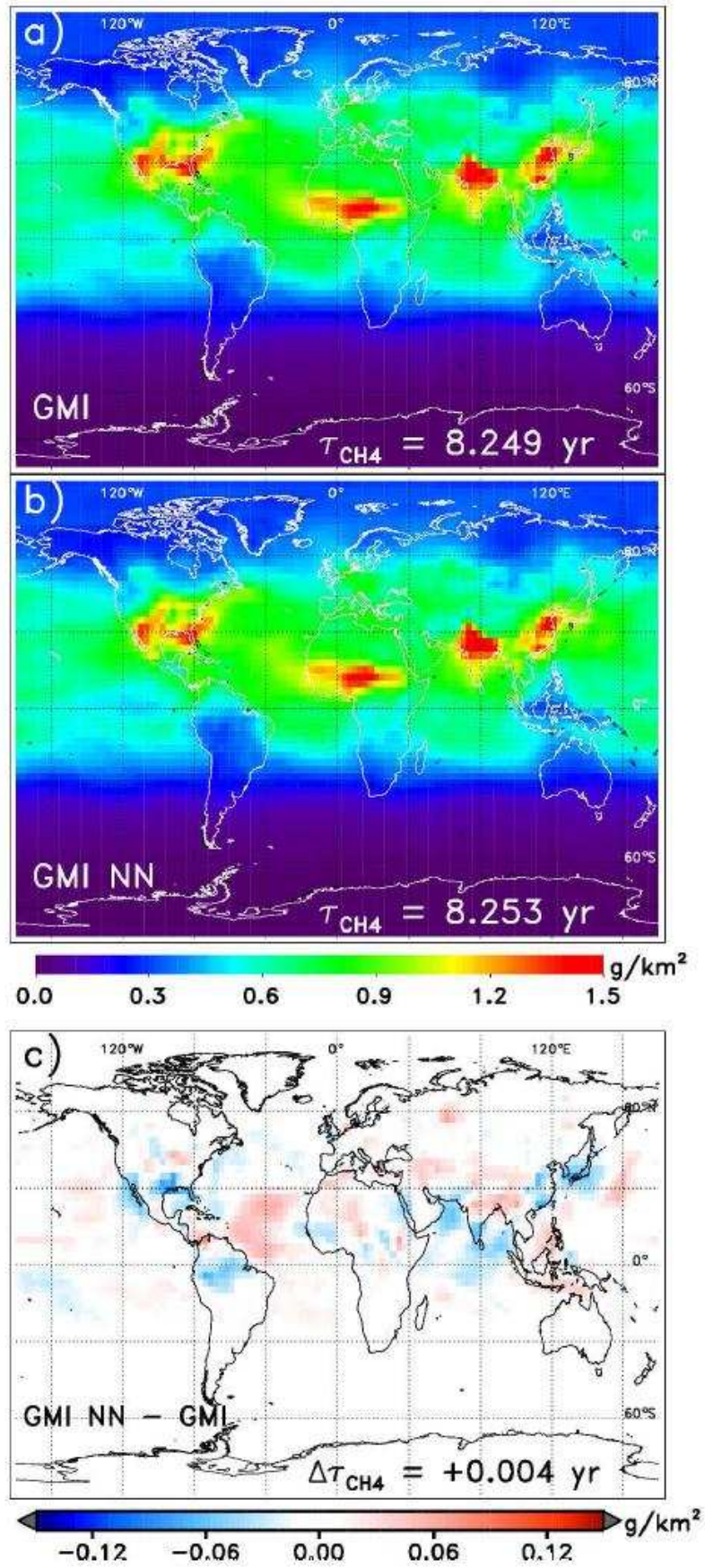


Figure 3. Tropospheric OH mass columns calculated directly from GMI CTM output (panel a) and from GMI NN output generated from input of OH precursors from the GMI CTM (b) are shown for July. The CH_4 lifetime (τ_{CH_4}) calculated for each 3-D OH distribution is indicated in the lower right corner of panels (a) and (b). The absolute difference in OH mass columns between panels (a) and (b) is shown in panel (c) as NN-CTM. The difference in τ_{CH_4} ($\Delta\tau_{\text{CH}_4}$), NN-CTM, is indicated in the bottom right corner of panel (c).

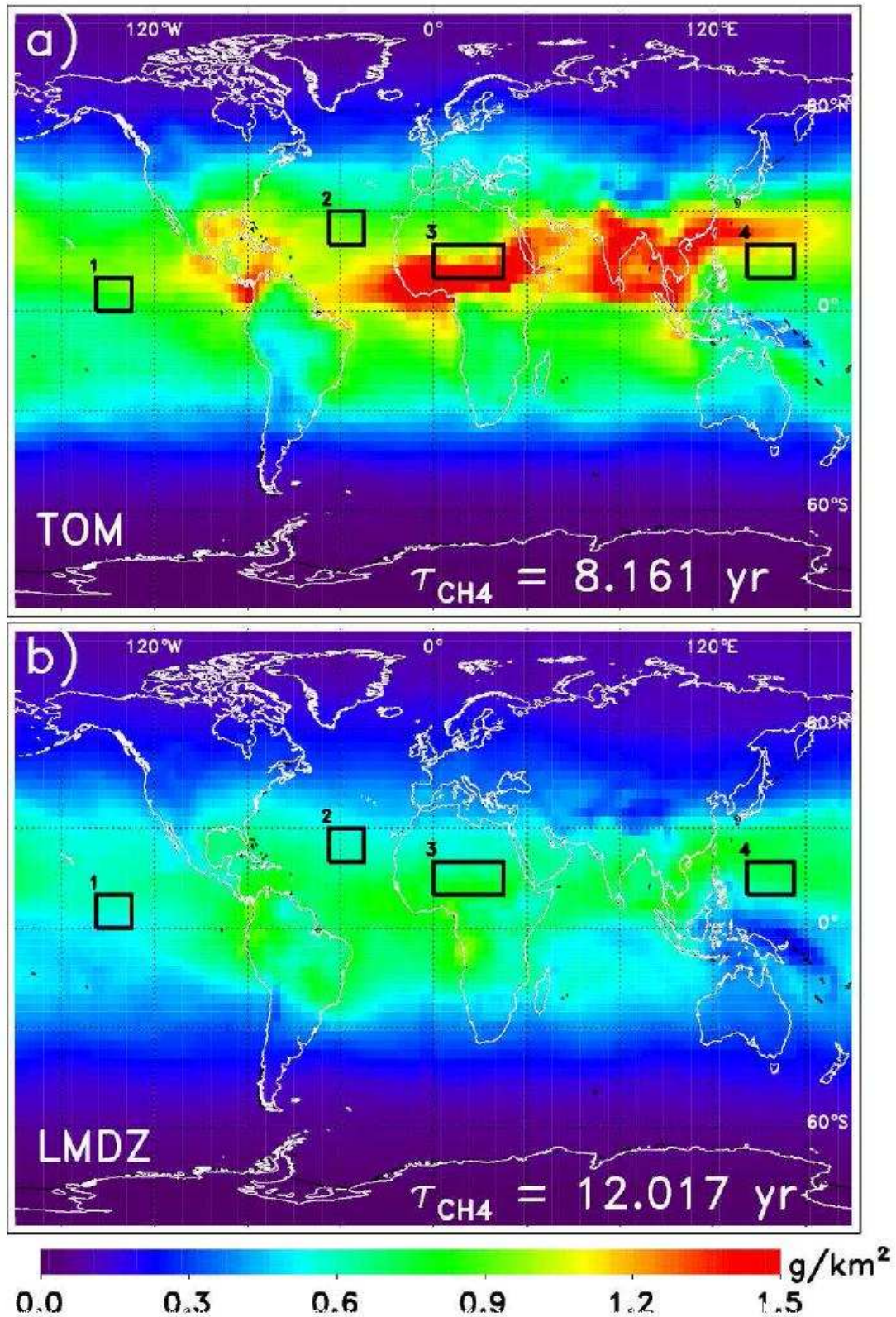


Figure 4. Tropospheric OH mass columns from TOMCAT (panel a, lowest value of τ_{CH_4}) and LMDz-INCA (b, highest value of τ_{CH_4}) for the month of April. Boxes highlight the geographical regions used for the box model evaluation of CTM chemical mechanism differences: Eastern Pacific (box 1), Atlantic (2), Africa (3), and Western Pacific (4).

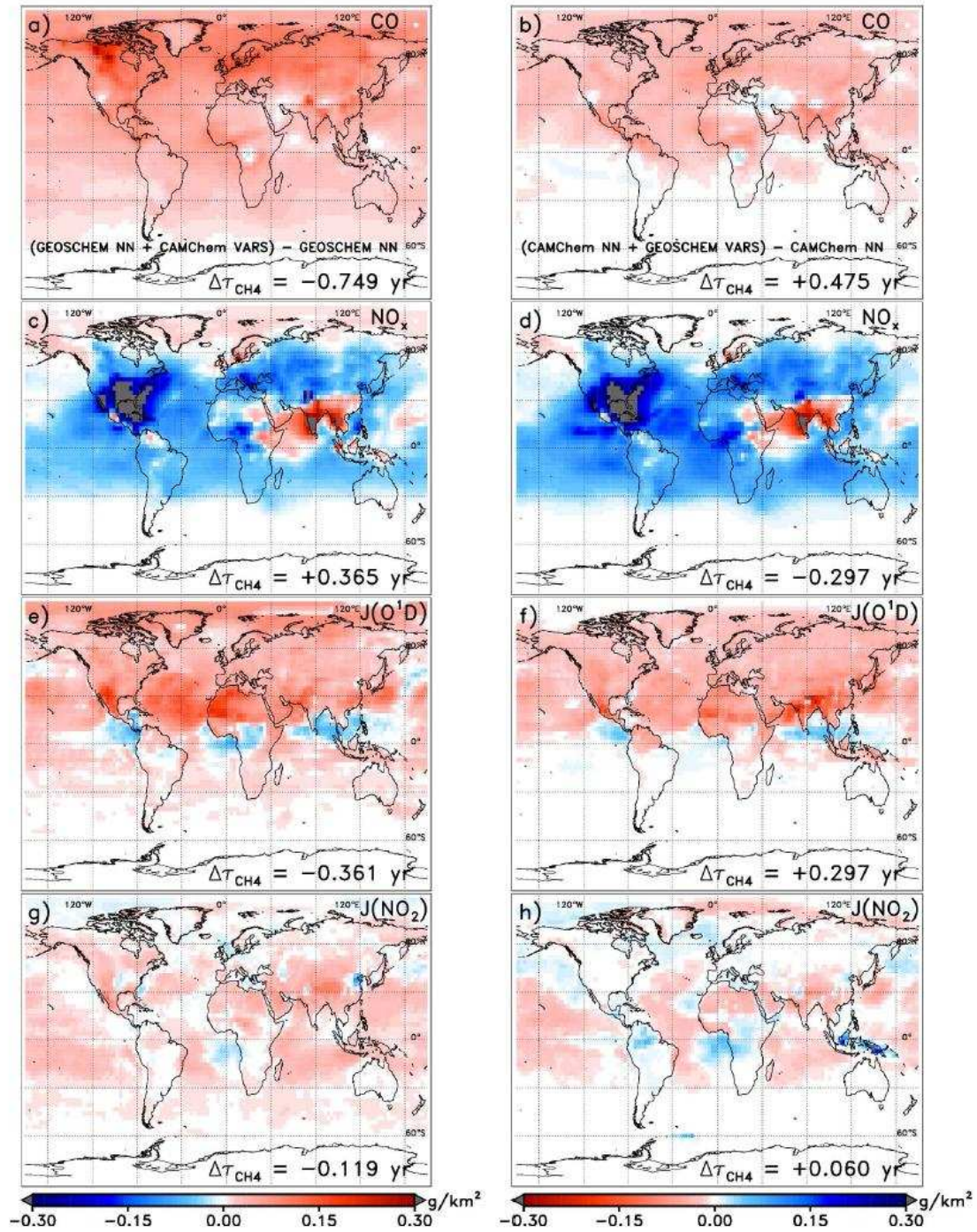


Figure 5. Tropospheric column mass OH differences for various inputs swapped between GEOS-Chem and CAM-Chem NNs. Left shows OH differences from GEOS-Chem's NN arising as a result of replacing CO (panel a), NO_x (c), $J(\text{O}_3 \rightarrow \text{O}(^1\text{D}))$ (e), and $J(\text{NO}_2)$ (g), from top to bottom, with that from CAM-Chem; right shows the same species swaps from GEOS-Chem into the CAM-Chem NN (panels b, d, f, h). The difference in τ_{CH_4} between the swap run and the base run of the NN is inscribed in the lower right corner of each plot. Note color bars are reversed between the left and right panels to highlight that OH increases in the NN of one model generally accompany OH decreases in the NN of the other model for a given variable swap.

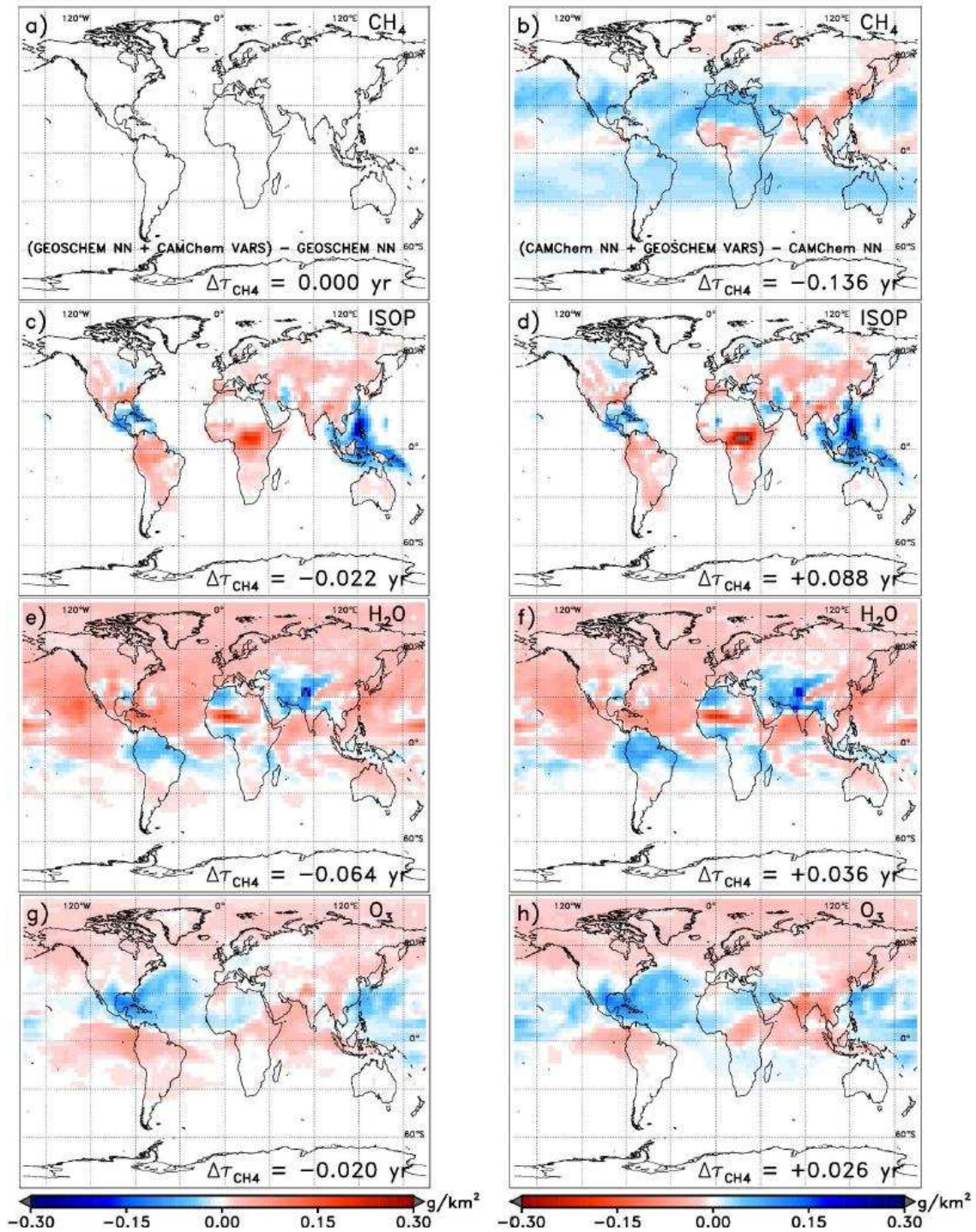


Figure 6. Same as Figure 5 except for swaps between the variables CH_4 (panels a and b), isoprene (c, d), H_2O (e, f), and O_3 (g, h), from top to bottom. Note color bars are reversed between the left and right panels to highlight that OH increases in the NN of one model generally accompany OH decreases in the NN of the other model for a given variable swap.

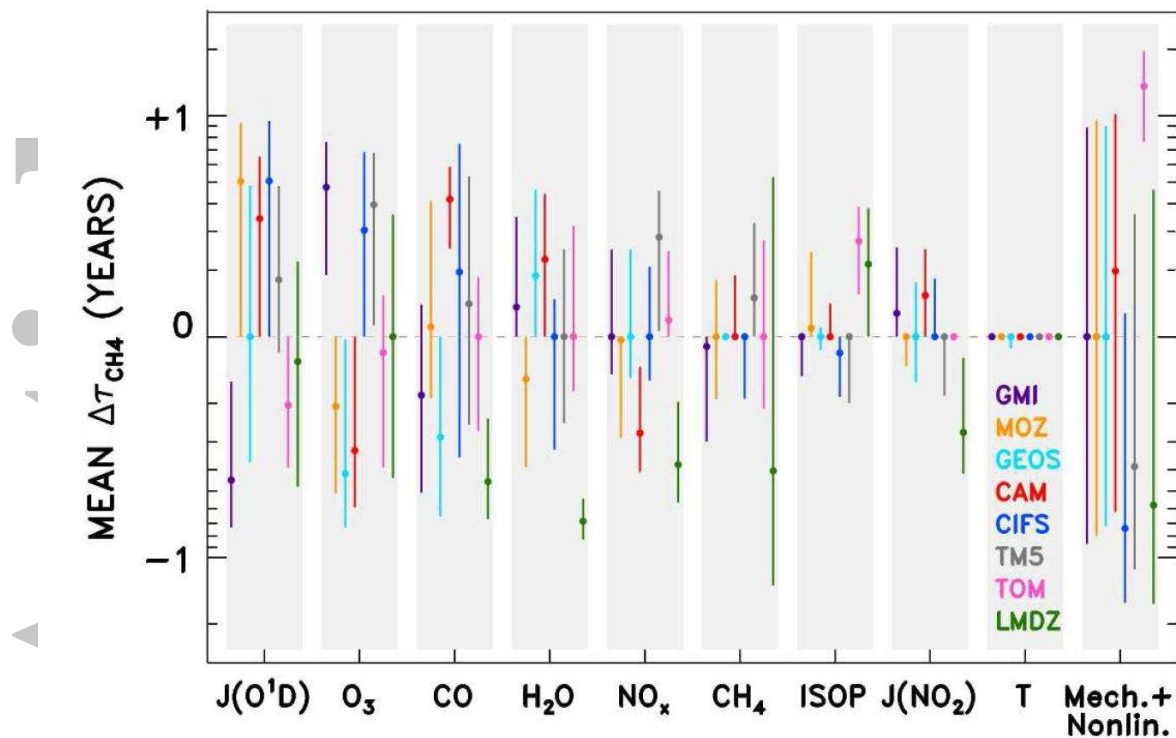


Figure 7. Changes in τ_{CH_4} as a result of exchanging the designated variable between all models, averaged over all four months analyzed here (January, April, July, October). “Mech.+Nonlin.” represents the difference between parent CTM τ_{CH_4} values not accounted for by the sum of $\Delta\tau_{\text{CH}_4}$ values for each variable (refer to Section 3.2 for more information). Ranking of inputs along the x-axis occurs in descending order of mean absolute value of $\Delta\tau_{\text{CH}_4}$ for all models, except for “Mech.+Nonlin.” which is listed last due to its origin as a remainder term. Error bars are standard deviations about the mean of all variable swaps between the indicated model and all other models.

Accepted

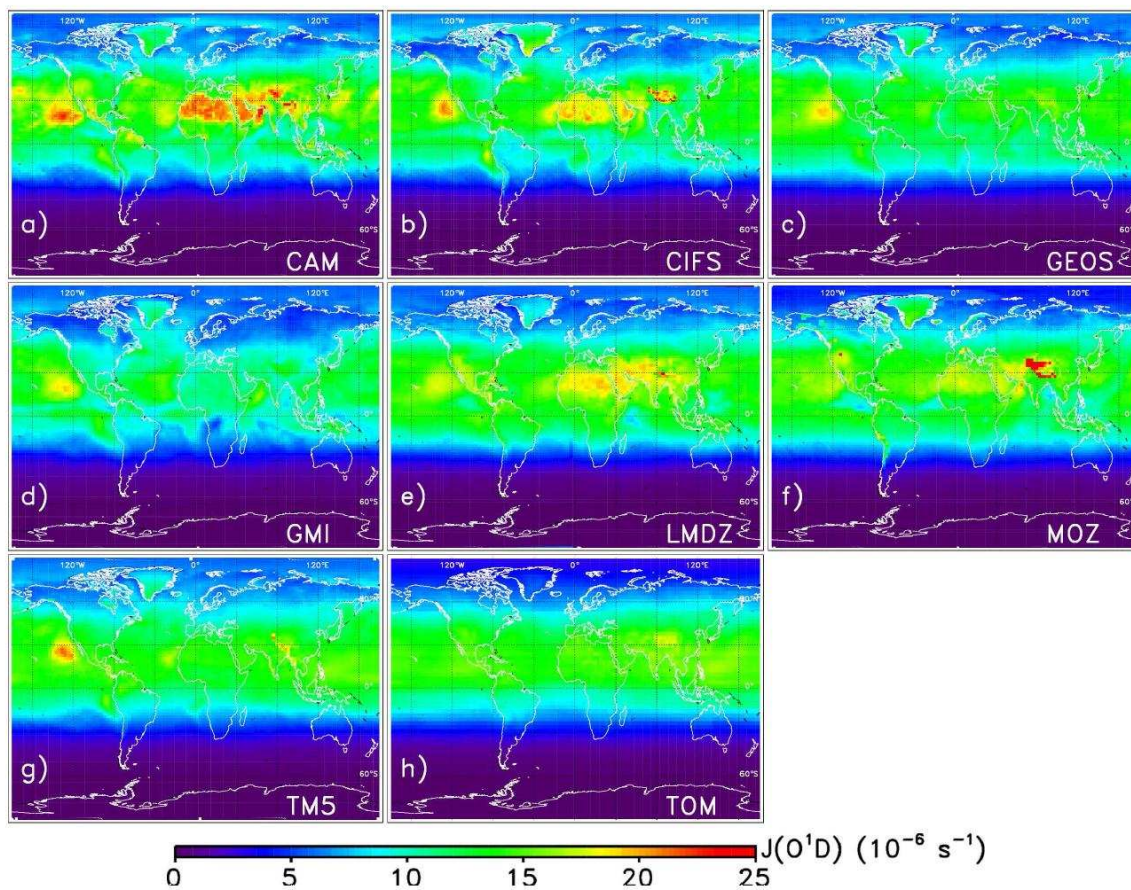


Figure 8. Monthly mean fields of $J(\text{O}_3 \rightarrow \text{O}(^1\text{D}))$ for July at pressure level closest to 850 hPa for the eight POLMIP CTMs: CAM-Chem (panel a), C-IFS (b), GEOS-Chem (c), GMI (d), LMDz-INCA (e), MOZART-4 (f), TM5 (g), and TOMCAT (h).

Accepted

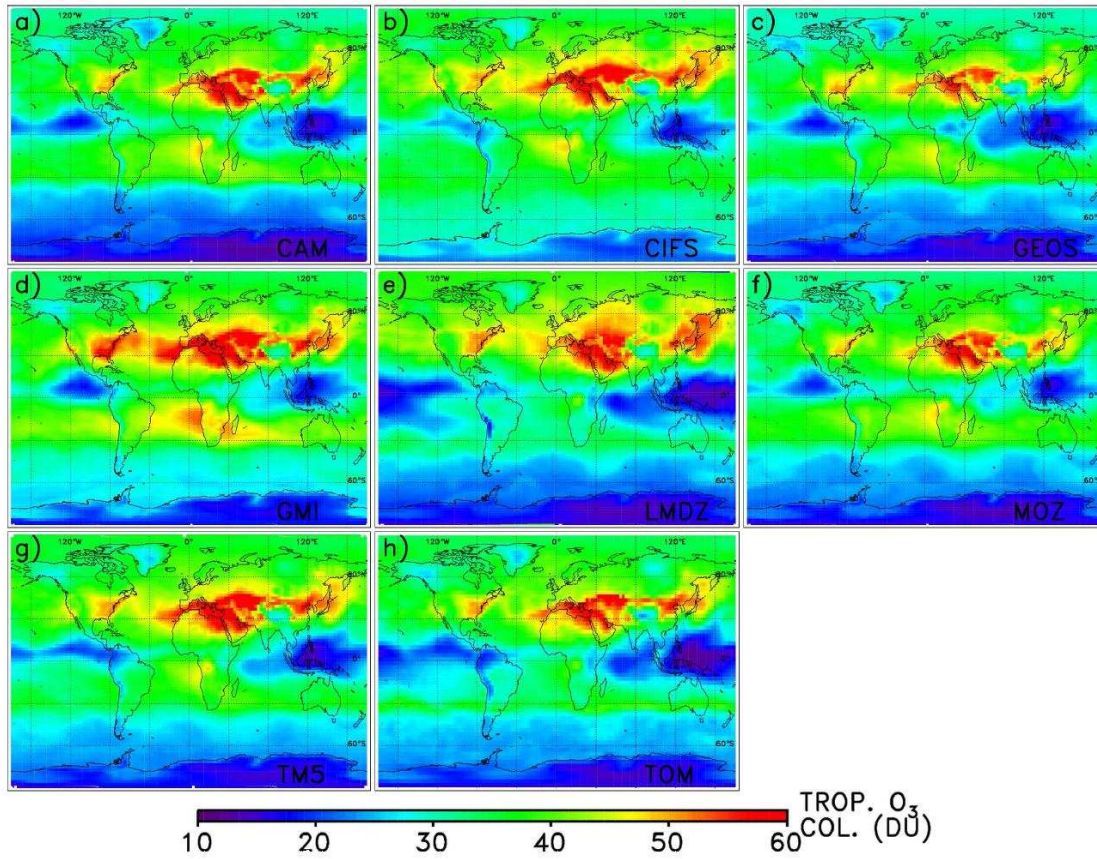


Figure 9. Monthly mean tropospheric O₃ columns in July for the eight POLMIP CTMs: CAM-Chem (panel a), C-IFS (b), GEOS-Chem (c), GMI (d), LMDz-INCA (e), MOZART-4 (f), TM5 (g), and TOMCAT (h). Tropopause pressures were calculated for individual models using a chemical tracer definition as defined in Pan et al., [2004].

Accept

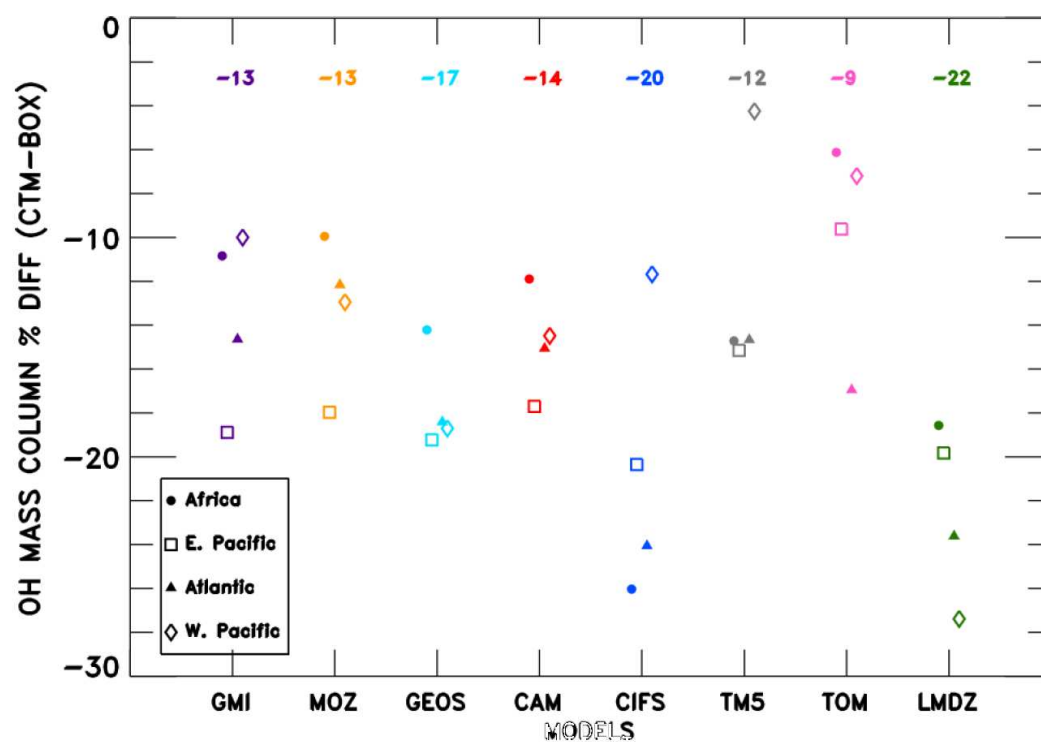


Figure 10. Percent difference in the tropospheric OH mass column values calculated by individual CTMs and the DSMACC box model (CTM-BOX), constrained to monthly mean values of the NN inputs CO, O₃, CH₄, H₂O, and isoprene as well as the NN inputs NO, J(O₃→O(¹D))), and J(NO₂) scaled to represent instantaneous noon-time values following the method Nicely et al., [2016] for the geographic region indicated. Additional VOCs ethane (C₂H₆), propane (C₃H₈), acetone (CH₃COCH₃), acetaldehyde (CH₃CHO), and formaldehyde (HCHO) not used in the NN analysis are also used to constrain the box model (with the exception that acetone was not output from C-IFS and is excluded from box model analysis of that CTM). The numbers shown along the top axis of the plot are the average percent difference in OH mass columns across all four regions for the individual CTMs.

Accepted